Pathway-specific responses of isoprene-derived secondary organic aerosol formation to anthropogenic emission reductions in a megacity in eastern China

Huilin Hu[1], Yunyi Liang[2], Ting Li[2], Yongliang She[2], Yao Wang[1,3], Ting Yang[1], Min Zhou[4], Ziyue Li[1], Chenxi Li[1], Huayun Xiao[1], Jianlin Hu[2], Jingyi Li[2,*], Yue Zhao[1,*]

[1]School of Environmental Science and Engineering, Shanghai Jiao Tong University, Shanghai 200240, China

[2]Jiangsu Key Laboratory of Atmospheric Environment Monitoring and Pollution Control, Collaborative Innovation Center of Atmospheric Environment and Equipment Technology, School of Environmental Science and Engineering, Nanjing University of Information Science and Technology, Nanjing 210044, China

[3]Ningbo Ecological and Environmental Monitoring Center, Ningbo 315012, China,

[4]State Environmental Protection Key Laboratory of the Cause and Prevention of Urban Air Pollution Complex, Shanghai Academy of Environmental Sciences, Shanghai 200233, China

Correspondence: Yue Zhao (yuezhao20@sjtu.edu.cn); Jingyi Li (Jingyili@nuist.edu.cn)

ABSTRACT:Isoprene-derived secondary organic aerosol (iSOA) represents a major biogenic source of atmospheric OA, with its formation strongly influenced by anthropogenic emissions. However, long-term iSOA measurements in polluted urban regions remain scarce, limiting the understanding of anthropogenic influences on iSOA formation. In this study, field observations of iSOA were conducted in Shanghai, China during summers and winters of 2015, 2019, and 2021, aiming to assess the iSOA response to emission reductions over this period. The particulate iSOA tracers, formed via reactive uptake of isoprene-derived epoxides, were measured by gas chromatography-mass spectrometry and high-resolution liquid chromatography-mass spectrometry. After accounting for the measurement uncertainties, both total iSOA and organosulfates (OSs) tracers (including 2-methyltetrol sulfates and 2-methylglyceric acid sulfate) decreased annually, while summertime polyol tracers like 2-methyltetrols (2-MTs) and 2-methylglyceric acid (2-MG) varied insignificantly despite strong NOx reductions. Declining aerosol reactivity toward isoprene-derived epoxides and reduced atmospheric oxidizing capacity drove the decrease in OSs but could not explain the trend of summertime polyols. Simulations with the Community Multiscale Air Quality model in 2015 and 2019 captured the decrease in total iSOA and OSs, confirming a driving role of chemical processes. However, the model failed to replicate relatively stable polyol levels in summer, suggesting additional factors (e.g., potential unaccounted sources of 2-MTs and methacrolein, the precursor to 2-MG) may buffer their variations. These findings highlight pathway-specific iSOA responses to emission reductions in a megacity and the importance of targeted anthropogenic emission reductions for mitigating biogenic SOA formation through regulating atmospheric oxidizing capacity and aerosol reactivity.

1. Introduction

Isoprene (2-methyl-1,3-butadiene, C_5H_8), mainly emitted by terrestrial vegetation, represents the largest source of atmospheric non-methane hydrocarbons, with a global emission flux of 500-750 Tg yr^{-1} (Guenther et al., 2006). Because of its large abundance and high reactivity, the oxidation of isoprene contributes significantly to the formation of secondary organic aerosol (SOA) in the troposphere, estimated to 19.6 TgC yr^{-1} (Kelly et al., 2018). The formation chemistry of isoprene-derived SOA (iSOA) has been extensively studied in laboratory, field, and modelling studies, which have shown that anthropogenic pollutants such as nitrogen oxides (NO_x) and sulfur dioxide (SO_2, the precursor to particulate sulfate) play a crucial role in the formation of iSOA (Shrivastava et al., 2019).

Photooxidation is the dominant fate of isoprene in the atmosphere, during which the C=C bond of isoprene is initially attacked by OH radicals to produce an alkyl radical (Teng et al., 2017), followed by the formation of isoprene hydroxyperoxy radicals ($ISOPO_2$) via oxygen addition (Surratt et al., 2010). The fate of $ISOPO_2$ radicals depends on the environmental conditions. When the NO_x level is sufficiently low (referred to as HO_2-dominated conditions), $ISOPO_2$ would mainly react with HO_2 radicals to form hydroxyhydroperoxides (ISOPOOH) (Paulot et al., 2009). Further OH radical addition to ISOPOOH produces isomeric isoprene epoxydiols (IEPOX, trans-β-IEPOX: cis-β-IEPOX = 0.63:0.37) with a yield of ~70-80% (Paulot et al., 2009; Bates et al., 2014; St. Clair et al., 2016). The gaseous IEPOX can be taken up into aqueous aerosol and undergo acid-catalyzed reactions to form polyols, organosulfates (OSs), and oligomers (Hettiyadura et al., 2019; Lin et al., 2012; Surratt et al., 2010). Several constituents including 2-methyltetrols (2-MTs) and their oligomers, C_5-alkene triols, methyl tetrahydrofurans, and 2-methyltetrol sulfates (2-MT-OS), which were extensively measured in both laboratory-generated and ambient SOA (Xu et al., 2015; Isaacman-Vanwertz et al., 2016; Surratt et al., 2010; Surratt et al., 2007; Worton et al., 2013; Yee et al., 2020), have been employed as molecular tracers of SOA derived from reactive uptake of IEPOX (IEPOX-SOA).

When the NO_x level is high (referred to as NOx-dominated conditions), $ISOPO_2$ would preferentially react with NO, producing unsaturated carbonyls such as methacrolein (MACR) and methyl vinyl ketone (MVK). A large fraction (~45%) of MACR can be further oxidized by OH radicals via aldehydic H-abstraction, followed by oxygen addition to form an acylperoxy radical, $MACRO_2$

69 (Orlando et al., 1999). Subsequent reaction between $MACRO_2$ and NO_2 yields MPAN, which was

70 proposed to form hydroxymethyl methyl-α-lactone (HMML) or methacrylic acid epoxide (MAE) (Lin

71 et al., 2013; Nguyen et al., 2015). Both of these two epoxides can undergo heterogeneous acid-catalyzed

72 reactions to form 2-methylglyceric acid (2-MG) as well as its oligoesters and sulfated derivatives (2-

73 methylglyceric acid sulfate, 2-MG-OS), which serve as the molecular tracers of HMML&MAE-derived

74 SOA (Kjaergaard et al., 2012; Lin et al., 2013).

75   In addition to altering the fate of RO_2 (including $ISOPO_2$ and $MACRO_2$), NO_x also plays an

76 essential role in regulating atmospheric oxidizing capacity (e.g., the OH level), which governs the

77 photooxidation rate of isoprene in the atmosphere. Compared to NOx that strongly affect the gas-phase

78 oxidation chemistry of isoprene, sulfate aerosol mainly exerts influences on the multiphase chemistry

79 of isoprene-derived epoxides. On one hand, sulfate serves as an important nucleophile in the reactive

80 uptake of isoprene epoxides to form OSs, which competes with the reaction of epoxides with water (Lin

81 et al., 2013). On the other hand, sulfate can alter the physicochemical properties of particles such as

82 liquid water content (LWC), acidity, and phase state (Xu et al., 2016; Pye et al., 2017), which are the

83 key factors influencing the multiphase reactivity of epoxides and the formation of iSOA.

84   Because of the complexity in the gas-phase and multiphase chemistry leading to iSOA formation,

85 the product distribution of HO_2- versus NO_x-dominated pathways as well as their dependence on

86 different influencing factors (i.e., NOx, sulfate, LWC, and aerosol acidity) varies significantly in

87 different environments. A number of field measurements have found that the formation of IEPOX-SOA

88 tracers was predominated over the HMML&MAE-SOA tracers, even in some NO_x-rich urban areas

89 (Zhang et al., 2022; Hu et al., 2008; Yee et al., 2020), while a few studies showed that the production

90 of HMML&MAE-SOA was more prevalent, e.g., in Tianjin, China (Fan et al., 2020) and urban areas

91 of California (Lewandowski et al., 2013). Sulfate was found to be the primary driver of isoprene-derived

92 SOA in rural and urban regions as the iSOA correlated strongly with sulfate while such correlation did

93 not occur with LWC and pH, e.g., in central Amazonia and southeastern U.S (Xu et al., 2015; Yee et al.,

94 2020). It should be noted that significant uncertainties exist in the quantification of iSOA tracers in

95 ambient aerosols due to the lack of authentic standards and/or the presence of measurement artifacts

96 (e.g., matrix effects) (Fu et al., 2012; Wang et al., 2008; Ding et al., 2014; Fu et al., 2016; Fu et al.,

97 2014; Fan et al., 2020; Zhong et al., 2021). Furthermore, while the iSOA polyol tracers are formed in

98 the particle phase, they can actively partition between gas and particle phases due to their semi-volatile

99 characteristics (Fan et al., 2020; Isaacman-Vanwertz et al., 2016; Nguyen et al., 2015). As a result,

100 considering their particle-phase concentration only may bias our understanding of the atmospheric

101 abundance and chemistry of iSOA.

102   In recent years, great changes have taken place in air pollutant emissions, atmospheric composition,

103 and air quality in China due to the implementation of stringent clean air policies nationwide. For

104 example, $PM_{2.5}$ mass concentrations dropped significantly, with a notable reduction in inorganic water-

105 soluble ions such as sulfate, ammonium, and cations (Liu et al., 2023a; Zheng et al., 2018; Liu et al.,

106 2023b; Geng et al., 2024), and a relatively small decrease in organic aerosol in eastern China in the past

107 decade (Liu et al., 2023a; Yao et al., 2023). The reduction of inorganic ions including sulfate and non-

108 volatile cations (Na^+, K^+, Ca^{2+} and Mg^{2+}) resulted in a significant decrease in LWC and a slight increase

109 in aerosol acidity in this region (Zhou et al., 2022). However, concentrations of VOCs and ozone

110 exhibited different trends, with a slight decrease for the former while the latter showing an upward trend

111 before 2018 and a slight declining trend after 2018 (Wang et al., 2022; Liu et al., 2023a; Yao et al., 2023;

112 Gong et al., 2025). The changing atmospheric conditions can affect both gas-phase and particle-phase

113 chemistry, as well as the gas-particle partitioning behavior of organics. However, how the formation of

114 biogenic SOA, such as iSOA, respond to the changes in anthropogenic emissions and air pollution

115 conditions in polluted regions remains poorly understood.

116   The aim of this study is to understand the atmospheric abundance and formation mechanisms of

117 iSOA under the influence of continuous anthropogenic emission reductions in eastern China. Ambient

118 $PM_{2.5}$ samples were collected at an urban site in megacity Shanghai in winter and summer of 2015,

119 2019, and 2021. The concentrations of isoprene-derived polyols and OSs from both HO_2- and NO_x-

120 dominated pathways in $PM_{2.5}$ samples were measured using gas chromatography-mass spectrometry

121 (GC-MS) and high-resolution liquid chromatography-mass spectrometry (LC-MS), respectively, with

122 the aid of a suite of authentic and surrogate standards. The quantification errors of iSOA tracers were

123 evaluated and their gas-particle partitioning behaviors were considered. The relative distribution of

124 measured iSOA tracers from different pathways as well as their inter-annual and seasonal variations

125 were analyzed and compared to the calculated reaction efficiency of different pathways as well as the

126 simulated values using the Community Multiscale Air Quality (CMAQ) model, which helps to constrain

127 the formation mechanisms of iSOA and the key factors driving the inter-annual variation of iSOA tracers.

2. Materials and methods

2.1 Sampling and Chemical Analysis

130 Ambient $PM_{2.5}$ samples were collected on the rooftop of a 20-m tall teaching building at Xuhui

131 Campus of Shanghai Jiao Tong University (31.201° N, 121.429° E) located in the urban center of

132 Shanghai, China. The site is impacted by a mixed commercial and residential area. The sampling

133 campaigns were conducted in summer (July 14 to August 9 in 2015; 14 July to 9 August 2019; 7 July

134 to 5 August 2021) and winter (6 January to 26 January 2016; 27 December 2018 to 16 January 2019;

135 22 December 2021 to 18 January 2022) of 2015, 2019, and 2021. Sampling started at 8:00 am local

136 time and lasted for 23 hours. A total of 138 $PM_{2.5}$ samples were collected on prebaked (550 ℃, 6 h)

137 quartz filters (18 × 23 cm^2, Whatman) using a high-volume sampler (HiVol 3000, Ecotech) at a flow

138 rate of 67.8 m^3 h^{-1}. All sampled filters were wrapped with prebaked aluminum foil and stored at -20 ℃

139 until analysis.

140 iSOA polyol tracers, included 2-MG, cis-2-methyl-1,3,4-trihydroxy-1-butene, trans-2-methyl-

141 1,3,4-trihydroxy-1-butene, and 3-methyl-2,3,4-trihydroxy-1-butene (cis-2-MTB, trans-2-MTB, and 3-

142 MTB, collectively named as C_5-alkene triols), as well as 2-methylthreitol and 2-methylerythritol

143 (collectively named as 2-MTs), were analyzed by a GC-MS. The details regarding the sample

144 preparation and analysis protocol are presented in Section S1 in the supplement. An example of the total

145 ion chromatograms (TIC) of iSOA polyol tracers is shown in Figure S1d. For iSOA polyol tracers,

146 surrogate standards including erythritol, ketopinic acid, and glycerol were used for quantifications in a

147 number of studies (Kang et al., 2018; Ding et al., 2014; Zhang et al., 2019; Fan et al., 2020). In this

148 study, concentrations of 2-MG and 2-methylerythritol were quantified using their authentic standards

149 (Toronto Research Chemicals, 99.8%), and C_5-alkene triols and 2-methylthreitol were quantified by 2-

150 methylerythritol. The uncertainty for C_5-alkene triols was estimated previously and their concentration

151 was found to be underestimated by 65% when 2-methylerythritol was used as the surrogate

152 standard(Frauenheim et al., 2022). Furthermore, the uncertainty of 2-methylthreitol quantified by 2-

methylerythritol was assumed to be negligible as the differences in the TIC response for homologues
are determined by carbon number, functional groups, and number of active hydrogen atoms that would
silylate (Stone et al., 2012).

The particulate iSOA OSs were analyzed by a LC-MS employing a reversed-phase column (C_{18}, 2.1 mm ×100 mm, 1.7 μm, Waters). The sample extraction procedure and analysis protocol were described in detail in our previous work (Wang et al., 2021). A brief summary is given in Section S2 and examples of total and extracted ion chromatograms of iSOA OSs are provided in Figure S1a-c. The lactic acid sulfate (LAS) was used as a surrogate standard to quantify the 2-MT-OS and 2-MG-OS. Use of surrogate standards would lead to uncertainties in measured concentrations of 2-MT-OS and 2-MG-OS (Bryant et al., 2020; Bryant et al., 2021), but not alter the inter-annual trend of iSOA OSs.

2.2 Additional measurements and models

The concentrations of organic carbon (OC) and element carbon (EC) in filter samples were measured using a thermal–optical multiwavelength carbon analyzer (DRI, Model 2015). The concentration of organic mass (OM) was estimated by multiplying the OC by 1.6 (Tao et al., 2014). An ion chromatograph (Metrohm MIC) was employed to determine water-soluble inorganic compounds (e.g., sulfate, nitrate, chloride, ammonium, potassium ion, and calcium ion). Temperature, relative humidity (RH), as well as the concentrations of trace gases and $PM_{2.5}$ were measured at a state-controlled air quality monitoring station on the Xuhui Campus of Shanghai Normal University, which is surrounded by residential areas and commercial districts and 4.5 km southwest of the $PM_{2.5}$ sampling site of this work. The mean values of these meteorological parameters and pollutant concentrations are listed in Table S1.

LWC, pH, and bisulfate concentration in aqueous aerosols were predicted by the ISORROPIA-II thermodynamic model (Wang et al., 2021). The molar concentrations of particulate water-soluble inorganic ions (including sulfate, nitrate, chloride, ammonium, potassium ion, and calcium ion), temperature, and RH were input into the model, which was run in the forward mode for metastable aerosols. As the predicted aerosol pH could be underestimated when using particle-phase concentrations of ion species as inputs only (Hennigan et al., 2015), we adopted the pH values of 2015 and 2019 at a nearby site reported by Zhou et al. (2022), who used both particulate inorganic ion concentrations and

gaseous ammonia as inputs of ISORROPIA-II. Additionally, the 2021 pH was predicted by the ISORROPIA-II using particle-phase-only concentrations of ions as input due to lack of gas-phase NH_3 data. Previous studies have found that lacking gas-phase inputs of ammonia could lead to under-prediction of pH using thermodynamic equilibrium models, such as ISORROPIA and E-AIM (Guo et al., 2015; Song et al., 2018; Hennigan et al., 2015). Guo et al. (2015) found that the pH values were underestimated by 1 unit on average in southeast US when using only aerosol ammonium data as inputs in ISORROPIA model. Similarly, Song et al. (2018) found that a 10-fold increase in gas-phase NH_3 concentrations roughly corresponds to a 1 unit increase in pH in the ammonia-rich atmosphere like Beijing. In addition, we found that aerosol pH in 2015 and 2019 predicted using aerosol ammonium only as input in our study was on average 1 unit lower than that predicted using gas-plus-particle-phase ammonia as input in Zhou et al. (2022). Thus, we inferred that the lack of gas-phase concentrations of ammonia might lead to underestimation of pH by ~1 unit in the present study and increased the output pH estimated using aerosol ammonium only as input by one unit to represent aerosol acidity in 2021.

In addition, considering that iSOA polyol tracers are semi-volatile and water-soluble, which can partition into OM or dissolve into aerosol liquid water, their gas-phase and particle-phase fractions were estimated by accounting for the gas-organic phase partitioning using an organic absorptive equilibrium partitioning model and the gas-aqueous phase partitioning using the Henry's Law. The details of the estimation method are described in Section S3.

2.3 Quality control and quality assurance

Procedural blanks (run every 6 samples) and field blanks (two for each season) were extracted and analyzed in the same manner as the $PM_{2.5}$ filter samples. Target compounds were found below the detection limit in the blanks. The recovery of iSOA polyol tracers as represented by that of the internal standard (ketopinic acid) during GC-MS analysis was determined to be 85±17% and the recovery of iSOA OSs during LC-MS analysis was 72.5%, as determined using LAS spiked onto the filter in our previous study (Wang et al., 2021).

As the $PM_{2.5}$ sample extracts contain thousands of multifunctional compounds, there might exist a significant matrix effect in the analysis of iSOA tracers. The matrix effect of polyol tracers was evaluated by comparing the signal responses of authentic standards of 2-methylerythritol and 2-MG in

209   PM$_{2.5}$ extracts to those in pure solvent. Six filter samples representing low and high PM$_{2.5}$ concentrations

210   in summer and winter were used to test the matrix effect. 16 μL or 160 μL of 2-methylerythritol and 2-

211   MG standard mixtures (10 ppm) was added to the filter extracts to represent the low and high

212   concentrations of 2-methylerythritol and 2-MG in the samples. The filters were subsequently analyzed

213   as described in Section 2.1. The matrix factors of the standards were calculated as the ratio of their

214   signal response in sample extracts (the signal response of these species in non-spiked extracts was

215   subtracted) to their signal response in the pure solvent. As shown in Table S2, 2-MG had a matrix factor

216   of 0.77 ± 0.12, while that of 2-methylerythritol was 1.24 ± 0.08, indicating that the concentrations of 2-

217   MG were likely underestimated by 23% whereas 2-methylerythritol was overestimated by 24% due to

218   the matrix effect.

219   Previous studies have demonstrated that the concentrations of 2-MT-OS and 2-MG-OS were

220   significantly underestimated due to matrix effect by using reversed phase liquid chromatography-mass

221   spectrometry (RPLC-MS) (Hettiyadura et al., 2015; Bryant et al., 2020; Bryant et al., 2021). In the

222   present work, because of lack of authentic standards of isoprene-derived OSs, we are not able to

223   quantify the absolute value of underestimation in the concentration of 2-MT-OS and 2-MG-OS due to

224   the matrix effect. However, using ambient PM$_{2.5}$ samples with different concentrations, we can quantify

225   the relative extent of underestimation in OS concentrations due to matrix effect in different samples,

226   which allows for an evaluation of uncertainties in the abundance, trend, and relative ratios of different

227   iSOA tracers in this study. In the matrix effect experiments, the extracts of ambient PM$_{2.5}$ samples with

228   different concentrations were mixed and the measured signals of 2-MT-OS and 2-MG-OS in mixed

229   extracts were compared to the sum of OS signals detected separately in individual extracts. The

230   concentrations of PM$_{2.5}$, sulfate, as well as 2-MT-OS and 2-MG-OS in ambient samples used for this

231   evaluation are listed in Table S3. The relative matrix effect factor (F$_{matrix}$), defined as the ratio of the

232   measured OS signals in mixed extracts to the sum of OS signals measured in each extract before mixing,

233   are used to evaluate the matrix effect of OSs. A F$_{matrix}$ value of less than 1 indicates the presence of

234   matrix effect.

235   As shown in Figure S2, the F$_{matrix}$ values were significantly smaller than 1 in both summer and

236   winter, indicating that the signal responses of 2-MT-OS and 2-MG-OS in mixed extracts were largely

237 suppressed due to the matrix effect. Notably, F_{matrix} exhibits a significant negative dependence on the

238 reduced mass (μ, µg m^{-3}), a proxy used to represent effective mass loadings of the mixed PM$_{2.5}$ extracts,

239 defined as:

$$\mu = \sqrt{m_1 * m_2/(m_1 + m_2)} \tag{1}$$

241 where m_1 and m_2 are the PM$_{2.5}$ mass loading of individual samples. This observation suggests that the

242 concentrations of iSOA OSs in PM$_{2.5}$ samples collected in 2015 were underestimated more than those

243 in 2021, given that ambient PM$_{2.5}$ concentrations declined by 39.8% and 47.0% from 2015 to 2021 in

244 summer and winter, respectively.

245   As PM$_{2.5}$ concentrations in ambient samples used for the matrix effect evaluation generally

246 represent lower or upper ends of PM$_{2.5}$ concentrations during the observation period (see Table S3), the

247 relative differences in measured F_{matrix} values at varying reduced mass (Figure S2) may roughly reflect

248 the differences in the extent of underestimation in OS concentrations for samples collected across 2015-

249 2021. During summer, the F_{matrix} value decreased from 0.71 to 0.63 for 2-MT-OS and from 0.85 to 0.58

250 for 2-MG-OS with increasing reduced mass, indicating that the concentrations of these two iSOA OSs

251 were a factor of 1.2 and 1.5 more underestimated in 2015 than in 2021 due to matrix effect. Similarly,

252 during winter the F_{matrix} values of iSOA OSs decreased from 0.9 to 0.6 with rising reduced mass,

253 implying a factor of 1.5 greater underestimation in OS concentrations in 2015 than in 2021.

254 **2.4 Estimation of the reaction efficiency of isoprene-derived epoxides in aqueous aerosols**

255   The IEPOX/HMML/MAE can undergo acid-catalyzed nucleophilic addition with water and sulfate

256 to form polyol tracers (2-MTs and 2-MG) and OSs (2-MT-OS and 2-MG-OS) in aqueous aerosols,

257 respectively. The aqueous-phase pseudo-first-order rate constants (k_{aq}, s^{-1}) for epoxides could be

258 estimated by eq 1 (Eddingsaas et al., 2010),

$$k_{aq} = \sum_{i=1}^{N} \sum_{j=1}^{M} k_{ij} [nuc_i]_{aq} [acid_j]_{aq} \tag{2}$$

260 Where k_{ij} is the third-order reaction rate constant of isoprene-derived epoxides with nucleophile i

261 (water or sulfate) and acid j (hydrogen ion or bisulfate) in the aqueous phase and the reported values of

262 k_{ij} in previous studies are shown in Table 1. When epoxides react with water and sulfate, the aqueous-

263 phase reaction rate constants (k_{aq,H_2O} and $k_{aq,SO_4^{2-}}$) can be estimated by eqs 2 and 3, respectively.

264 $$k_{aq,\ H_2O}=k_{H_2O,H^+}[H_2O]_{aq}[H^+]_{aq}+k_{H_2O,HSO_4^-}[H_2O]_{aq}[HSO_4^-]_{aq} \tag{3}$$

265 $$k_{aq,\ SO_4^{2-}}=k_{SO_4^{2-},H^+}[SO_4^{2-}]_{aq}[H^+]_{aq}+k_{SO_4^{2-},HSO_4^-}[SO_4^{2-}]_{aq}[HSO_4^-]_{aq} \tag{4}$$

266 Where $[H^+]_{aq}$, $[HSO_4^-]_{aq}$, and $[H_2O]_{aq}$ are molar concentrations of hydrogen ion, bisulfate, and

267 ALWC in aqueous aerosols, which were estimated by ISORROPIA-II model, and $[SO_4^{2-}]_{aq}$ is the molar

268 concentration of sulfate.

269   The reactive uptake coefficient (γ) of epoxides on aqueous aerosols is parameterized by a resistor

270 model (Xu et al., 2016; Pye et al., 2013).

271 $$\frac{1}{\gamma}=\frac{1}{\alpha}+\frac{\omega}{4H_{epoxide}RT\sqrt{D_ak_{aq}}}\frac{1}{f(q)} \tag{5}$$

272 $$f(q)=\coth(q)-\frac{1}{q} \tag{6}$$

273 $$q=r_p\sqrt{k_{aq}/D_a} \tag{7}$$

274 Where r_p is the particle radius. Previous work has found that the surface area (S_a, m^2 m^{-3}) and volume

275 concentrations (V_a, m^3 m^{-3}) of dry PM$_{2.5}$ could be described as a function of PM$_{2.5}$ mass concentration

276 ($C_{PM_{2.5}}$, μg m^{-3}) in Shanghai (S_a=7.54×10^{-6}×$C_{PM_{2.5}}$+1.01×10^{-4}, V_a=5.59×10^{-13}×$C_{PM_{2.5}}$+1.02×10^{-12})

277 (Zang et al., 2022). In this study, the mean particle radius of dry PM$_{2.5}$ was calculated as $3V_a/S_a$, which

278 was then corrected for the aerosol hygroscopic growth to get the wet particle radius based on the κ-

279 Köhler hygroscopicity function (see details in Section S4). α is the mass accommodation coefficient

280 taking a value of 0.02 for both IEPOX and HMML&MAE (Mcneill et al., 2012), ω is the mean

281 molecular velocity of epoxides, H$_{epoxide}$ is the Henry's law constant in the aqueous phase, with a value

282 of 2.7 × 10^6 M atm^{-1} for IEPOX (Pye et al., 2013) and a constrained value of 7.5 × 10^6 M atm^{-1} for

283 HMML&MAE by CMAQ in Case 1, and k$_{aq}$ is the first-order reaction rate constant in the aqueous

284 phase (s^{-1}), estimated using eq 1.

285   To describe the overall loss rate of gas-phase epoxides due to the reactive uptake by aqueous

286   aerosols, the pseudo-first-order heterogeneous reaction rate constant was calculated by eq 7, when

287   neglecting the gas-phase diffusion limitation:

288   $$k_{het} = \gamma \omega S_a / 4 \tag{8}$$

289   **2.5 Model Simulations**

290   The CMAQ model (v5.2) was adopted to simulate the gas-phase concentration of isoprene and

291   particulate concentrations of 2-MTs, 2-MG, and their OS derivatives formed involving the reactive

292   uptake of IEPOX and HMML&MAE on aqueous aerosols (Pye et al., 2017) in both summer and winter

293   of 2015 and 2019 in Shanghai. The simulations performed with the standard CMAQ v5.2 are referred

294   to as the Base Case. While the advanced model simulations performed according to a recent study by

295   Zhang et al. (2023) are named as Case 1. In this advanced case, the iSOA polyol tracers were treated

296   as semi-volatile species that partition between gas, aqueous, and organic phases, while the OS tracers

297   were treated as non-volatile species. The removal of iSOA polyol tracers by OH radicals in the gas and

298   particle phases was also considered. The key parameters for simulating reactive uptake of

299   IEPOX/HMML&MAE and the removal of 2-MTs and 2-MG in the gas phase and aqueous aerosol in

300   the model are listed in Table S4 and S5.

301   In this work, three nested domains covering mainland China, eastern China, and the Yangtze

302   River Delta were configured with horizontal resolutions of 36 km × 36 km (d01), 12 km × 12 km (d02),

303   and 4 km × 4 km (d03), as shown in Figure S3. The outermost domain (d01) was driven by predefined

304   initial and boundary conditions from CMAQ, with its outputs supplying these conditions for d02,

305   which in turn provided them for d03. All domains employed a vertical structure consisting of 18 layers,

306   extending from the surface to an altitude of 21 km.

307   Anthropogenic emissions were sourced from the Multi-resolution Emission Inventory for China

308   (MEIC) version 1.4 for China (Geng et al., 2024) and the Regional Emission inventory in ASia (REAS)

309   version 3.2.1 for other Asian countries and regions (Kurokawa and Ohara, 2020). Open biomass

310   burning emissions were based on the Fire INventory from NCAR (FINN) version 2.5 (Wiedinmyer et

311   al., 2023). Biogenic emissions were estimated using the Model of Emissions of Gases and Aerosols

312   from Nature (MEGAN) version 2.1, incorporating the high-quality Leaf Area Index (HiQ-LAI) dataset

313 developed by Yan et al. (2024), which enhances the spatiotemporal consistency of MODIS LAI

314 products. Meteorology data was generated by the Weather Research and Forecasting (WRF) model

315 version 4.2.1 with initial and boundary conditions from the fifth generation ECMWF atmospheric

316 reanalysis data (ERA5).

317   The simulation was conducted for four periods: 12 July–9 August 2015, 25 December 2015–16

318 January 2016, 4–26 January 2019, and 12 July–5 August 2019. The first two days of each period were

319 treated as spin-up periods and excluded from the analysis.

3. Results and Discussion

3.1 Temporal evolution of major air pollutants during the observation period

322   Time series of $PM_{2.5}$ and its major components, as well as the major trace gases (NO_2 and O_3) and

323 meteorological parameters during the observation period are shown in Figure 1 and the seasonal and

324 inter-annual variations of various pollutants are further demonstrated in Figure 2. The concentration of

325 NO_2 exhibited an obvious downward trend, in particular in summer from 2015 to 2021, consistent with

326 a strong reduction in anthropogenic emissions during this period. By contrast, the concentration of O_3

327 significantly decreased from 52.0 ± 38.9 ppb in 2015 to 41.2 ± 22.8 ppb in 2019 ($p < 0.05$) and then

328 remained at a comparable level (43.4 ± 20.8 ppb) in 2021, suggesting a complex response of secondary

329 O_3 formation to primary emission reductions. During the observation period, the average $PM_{2.5}$

330 concentration decreased by 41.7% from 2015 to 2021, with concentrations of major components,

331 including sulfate, ammonium, and OM, decreasing by 51.8%, 40.6%, and 39.1%, respectively (Figure

332 2). In contrast, the concentration of nitrate showed a slight upward trend during this period, in line with

333 the measurement in urban Shanghai by Zhou et al. (2022). Overall, OM was the most abundant

334 component in $PM_{2.5}$, accounting for 10.2-72.7% (average 22.6%) of total $PM_{2.5}$ mass, followed by

335 sulfate (6.8-45.2%, average 17.7%), nitrate (0.5-32.6%, average 17.0%), and ammonium (1.1-18.2%,

336 average 8.8%). Ascribed to the strong decrease of inorganic ion concentrations (in particular sulfate),

337 aerosol LWC decreased from 9.14 ± 4.51 μg m^{-3} in 2015 to 4.40 ± 2.76 μg m^{-3} in 2021 ($p < 0.05$).

338 Aerosol pH decreased from 3.2 ± 0.4 in 2015 to 2.5 ± 0.9 in 2021 ($p < 0.05$), which was mainly driven

339 by the decrease of non-volatile cations during these years, though the decreased concentrations of

340 sulfate had an opposite effect on aerosol acidity (Zhou et al., 2022).
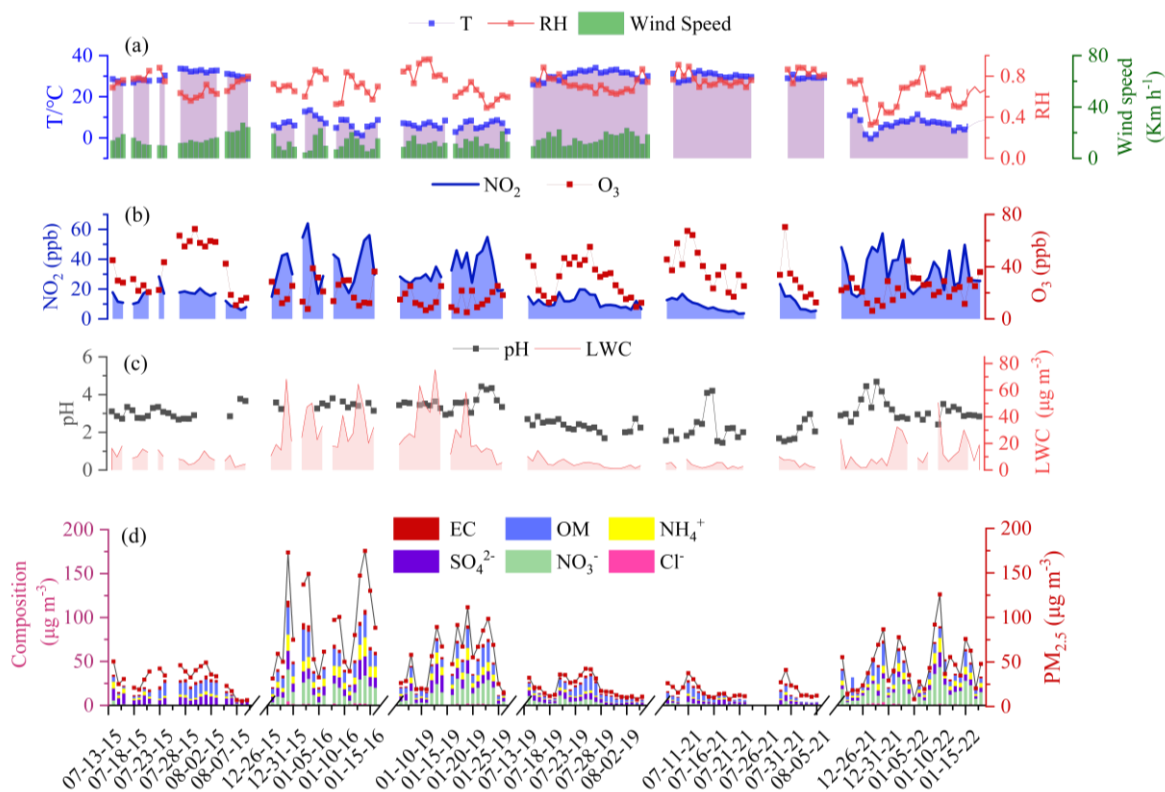
Figure 1. Temporal variations of (a) meteorological parameters (ambient temperature, relative humidity, and wind speed), (b) concentrations of NO_2 and O_3, (c) aerosol pH and liquid water content (LWC), and (d) concentrations of $PM_{2.5}$ and its major components (OM, EC, sulfate, nitrate, chloride, and ammonium) in urban Shanghai during the observation period. The wind speed data were not collected during the observations in 2021.

3.2 Seasonal and annual variations of iSOA tracers

The measured concentrations of particulate iSOA tracers during the observation period are summarized in Figure 2 and their specific concentration values are also provided in Table S1. Among the measured iSOA tracers, C_5-alkene triols were the most abundant species with average concentrations of 27.6 ng m^{-3} in 2015, 20.9 ng m^{-3} in 2019, and 11.1 ng m^{-3} in 2021, accounting for 28.8 %, 22.4, and 18.7 % of the total iSOA mass, followed by 2-MT-OS, 2-MTs, 2-MG-OS, and 2-MG. However, the concentrations of C_5-alkene triols might be overestimated since previous studies have reported that concentrations of C_5-alkene triols could be artifacts of thermal degradation products of 3-methyltetrahydrofuran-2,4-diols and 2-MT-OS during GC-MS analysis (Cui et al., 2018; Frauenheim et al., 2022). Frauenheim et al. (2022) found that less than 15% of 3-methyltetrahydrofuran-2,4-diols

357 could transfer to two isomers of C_5-alkene triols (cis-/trans-2-methyl-1,3,4-trihydroxy-1-butene). In the

358 present study, using 2-methylerythritol as a surrogate standard, the concentrations of 3-

359 methyltetrahydrofuran-2,4-diols were determined to be less than 5% of C_5-alkene triols in summer but

360 had comparable concentrations to C_5-alkene triols in winter. This result indicates that 3-

361 methyltetrahydrofuran-2,4-diols was a minor contributor to C_5-alkene triols in summer but an important

362 source for C_5-alkene triols in winter. In contrast, the contribution from the thermal degradation of 2-

363 MT-OS might be more significant, though the specific contribution remains to be quantified; Cui et al.

364 (2018) found that thermal degradation of 2-MT-OS could generate all three isomers of C_5-alkene triols,

365 while Yee et al. (2020) found that the thermal decomposition of 2-MT-OS could only produce one

366 isomer, 3-methyl-2,3,4- trihydroxy-1-butene. Given these uncertainties, it is difficult to quantitatively

367 evaluate the artifact formation of C_5-alkene triols during GC-MS analysis. Therefore, the abundance

368 and inter-annual trend of C_5-alkene triols were not discussed in detail in the present work.

369   As shown in Figure 2, the particle-phase concentrations of total and specific IEPOX-SOA tracers

370 (except 2-MTs) decreased yearly in both summer and winter between 2015-2021 (Figs. 2a-d), while the

371 particulate concentrations of total and specific HMML&MAE-SOA species did not show a significant

372 inter-annual trend in summer during this period (Figs. 2e-g). However, the inter-annual trend of iSOA

373 OSs could be altered due to the matrix effect. The measured concentration of 2-MT-OS exhibited a

374 decreasing inter-annual trend, while 2-MG-OS showed insignificant variation between 2015-2021.

375 Accounting for the significantly larger matrix effects in 2015 samples compared to 2021 samples (see

376 Section 2.3), the true concentrations of 2-MT-OS would decrease more sharply and 2-MG-OS might

377 also exhibit a declining trend. Recently, Frauenheim et al. (2024) demonstrated that gas-phase OH

378 oxidation of 3-methylenebutane-1,2,4-triol (3-MBT) and 3-methyltetrahydrofuran-2,4-diols, formed

379 from acid-catalyzed isomerization of IEPOX in aerosols, can yield 2-MT-OS and 2-MG-OS. However,

380 in the present study, the gas-phase concentrations of 3-MBT and 3-methyltetrahydrofuran-2,4-diols

381 were not measured, precluding a quantitative assessment of the contribution of their oxidation products

382 to 2-MT-OS and 2-MG-OS. Given that IEPOX-SOA concentrations observed here exhibited a

383 significant decreasing trend over the observation period, the concentrations of IEPOX isomerization

384 products, such as 3-MBT and 3-methyltetrahydrofuran-2,4-diols, likely also decreased annually.

385 Therefore, gas-phase OH oxidation of these species might represent a plausible contributor to the inter-

386 annual decline in 2-MT-OS and 2-MG-OS.

387
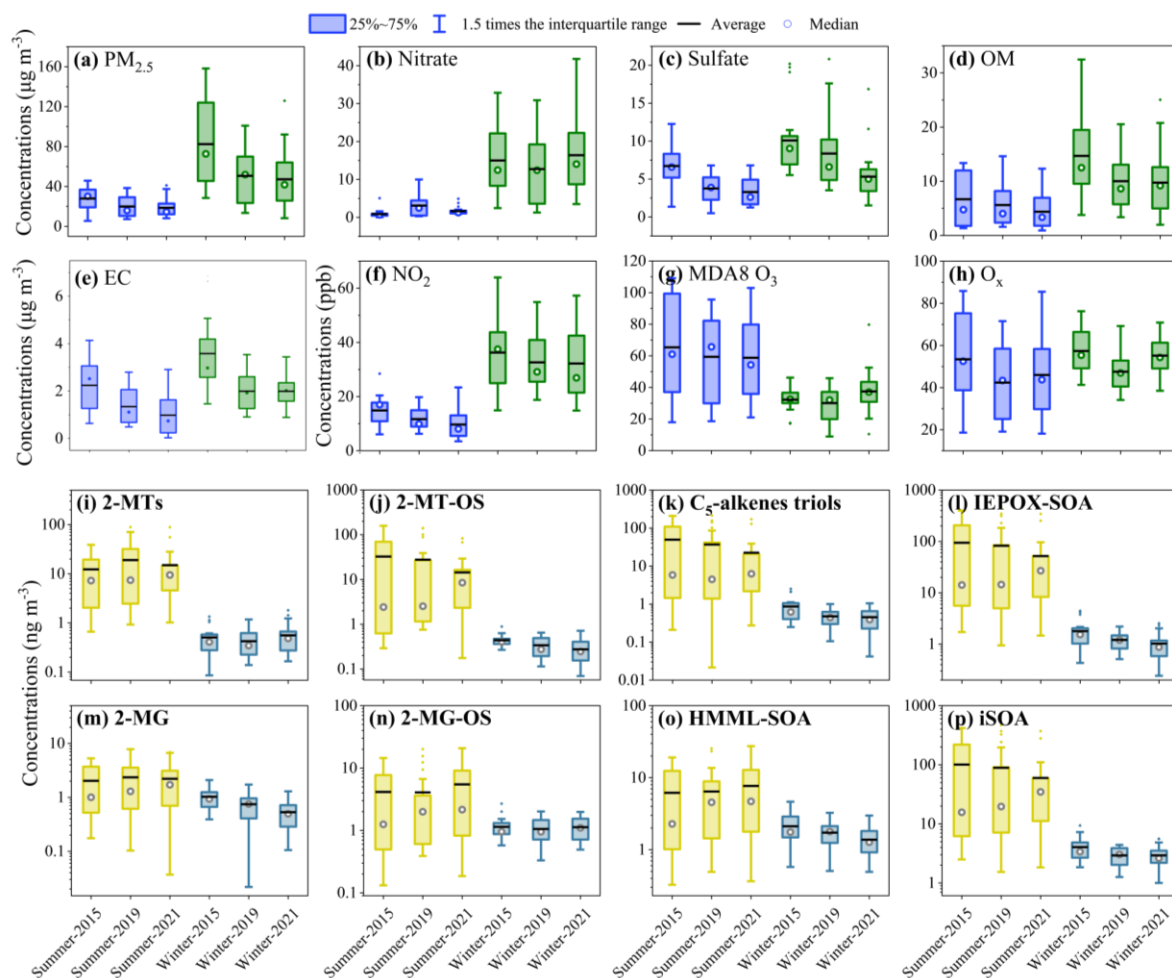
388 Figure 2. Seasonal and inter-annual variations concentration of PM$_{2.5}$ and its major components (a-e),

389 gas-phase anthropogenic pollutants (f-h), as well as particulate iSOA tracers, including (i)2-MTs, (j) 2-

390 MT-OS, (k) C$_5$-alkene triols, (l) IEPOX-SOA (the sum of 2-MTs, 2-MT-OS, and C$_5$-alkene triols), (m)

391 2-MG, (n) 2-MG-OS, (o) HMML&MAE-SOA (2-MG plus 2-MG-OS), and (p) iSOA (the sum of all

392 tracers).

393   The particulate concentrations of IEPOX-SOA (52.6 ± 97.6, 46.7 ±103.8, and 25.8 ± 62.9 ng m^{-3}

394 in 2015, 2019 and 2021, respectively) dominated over HMML&MAE-SOA (6.2 ± 6.4, 6.4 ± 7.0, and

395 7.7 ± 7.7 ng m^{-3}) in summer, while they were comparable to HMML&MAE-SOA in winter. Although

396 C$_5$-alkene triols might be largely artifacts of GC-MS analysis (Cui et al., 2018; Frauenheim et al., 2022),

397 the concentrations of IEPOX-SOA excluding C$_5$-alkene triols were still dominant over HMML&MAE-

398 SOA in summer. In addition, previous studies have demonstrated that the concentrations of 2-MT-OS

399   were underestimated more than 2-MG-OS by a factor of 5.7-9.1 in Beijing (Bryant et al., 2020) and 2.9

400   in Guangzhou (Bryant et al., 2021). If 2-MT-OS was also more significantly underestimated than 2-

401   MG-OS in the present study, the predominance of IEPOX-SOA over HMML&MAE-SOA would be

402   more pronounced. The dominance of IEPOX-SOA over HMML&MAE-SOA in summer is in

403   agreement with RPLC-MS measurements in Beijing, Hefei, and Kunming in China (Zhang et al., 2022)

404   and Birmingham, US (Rattanavaraha et al., 2016), as well as hydrophilic interaction liquid

405   chromatography-mass spectrometry (HILIC-MS) measurements conducted in urban Guangzhou, China

406   (Liu et al., 2025).

407   The annual average particulate concentration of the total iSOA polyol tracers (including 2-MTs, 2-

408   MG, and C_5-alkene triols) were 36.1 ± 63.3, 33.4 ± 70.5, and 18.7 ± 47.1 ng m^{-3} in 2015, 2019 and 2021,

409   higher than those of OS tracers (including 2-MT-OS and 2-MG-OS) by a factor of 2.5, 2.1, and 1.4,

410   respectively. However, given the significant underestimation of iSOA OSs due to matrix effect and

411   overestimation of C_5-alkene triols due to their potential artifact formation, the true concentration of

412   iSOA OSs would predominate over that of polyol tracers. The iSOA OSs prevailing over polyol tracers

413   is consistent with urban observations using HILIC-MS, such as in Manaus, Brazil (Cui et al., 2018) and

414   Guangzhou, China (Liu et al., 2025) (see Table S6). Using RPLC-MS, Bryant et al. (2020) also observed

415   higher concentrations of iSOA OSs than polyol tracers in Beijing, China. Considering the potential

416   underestimation of iSOA OSs due to matrix effect, the concentration of iSOA OSs would be even higher

417   than that of polyol tracers in their study.

418   2-MTs exhibited a different inter-annual trend compared to other IEPOX-SOA tracers (Figure 2i).

419   A possible explanation for this discrepancy is that 2-MTs may have origins other than reactive uptake

420   of IEPOX on aqueous aerosol. Previous studies have found that 2-methylerythritol, one isomer of 2-

421   MTs, could be generated by biosynthetic pathways (Duvold et al., 1997; Sagner et al., 1998; Rohmer,

422   1999; Lange et al., 2000; Yang et al., 2013). And the contributions of non-IEPOX pathway to 2-MTs

423   concentrations were pH-dependent, accounting for 20-40% in areas with aerosol pH < 2 and more than

424   70% under less acidic conditions (pH $\sim$ 2-5) (Zhang et al., 2023). The contribution of biological

425   emissions to 2-MTs might be important in Shanghai given its less acidic aerosol conditions (pH > 2).

426   As a whole, the particulate concentrations of iSOA decreased significantly in both seasons from 2015

427   to 2021. In addition, all iSOA compound classes had substantially higher concentrations in summer than

428   in winter. Such a strong seasonality in abundance is mainly driven by the higher temperature and

429   stronger solar radiation, and thereby more intensive isoprene emissions and photochemistry in summer

430   than in winter. Notably, HMML&MAE-SOA species exhibited a relatively smaller seasonal variation

431   than IEPOX-SOA. This is partially owing to the fast thermolysis of methacryloyl peroxynitrate (MPAN)

432   in summer, reducing the formation of HMML&MAE and thereby SOA (Worton et al., 2013).

433   To further investigate factors that affect the abundance of iSOA, the particulate concentrations of

434   2-MTs, 2-MT-OS, 2-MG, and 2-MG-OS, as well as the gas-phase concentration of isoprene were

435   simulated with the CMAQ model and compared to measurements in summertime and wintertime of

436   2015 and 2019 (see Figure 3). Predicted concentrations of isoprene were generally consistent with

437   observations with a median correlation (r^2=0.45), except in the summer of 2015, during which isoprene

438   concentrations were significantly overestimated (Figure 3a). For iSOA tracers, the Case 1 showed a

439   better prediction than the Base Case. Overall, the simulated IEPOX-SOA tracers were biased low in

440   summer, but biased high in winter (Figure 3b and 3c). In contrast, the 2-MG and 2-MG-OS were biased

441   low in both seasons (Figure 3d and 3e). The underestimation of 2-MG is consistent with previous

442   simulations at 14 sites across China in the summer of 2012 (Qin et al., 2018). Accounting for the

443   underestimation of OSs due to the matrix effect, simulated concentrations of 2-MT-OS would be more

444   biased low in summer but might be close to observations in winter. Similarly, the under-prediction of

445   2-MG-OS would be more significant in both seasons. The larger uncertainty of simulated

446   HMML&MAE-SOA tracers compared to that of IEPOX-SOA might be attributed to the lack of well

447   constrained kinetic parameters for reactive uptake of HMML and MAE. In addition, simulated

448   concentrations of iSOA tracer species had decreasing inter-annual trend in both Base Case and Case 1

449   (Figure S4), which was in agreement with observations of total iSOA, 2-MT-OS, and 2-MG-OS (with

450   matrix effect considered), but not for 2-MG and 2-MTs. These results suggest that the major factors

451   driving the overall formation and evolution of iSOA and in particular iSOA OSs were captured by the

452   model, while some factors governing the abundance of 2-MG and 2-MTs might not be well represented

453   in the model.

454
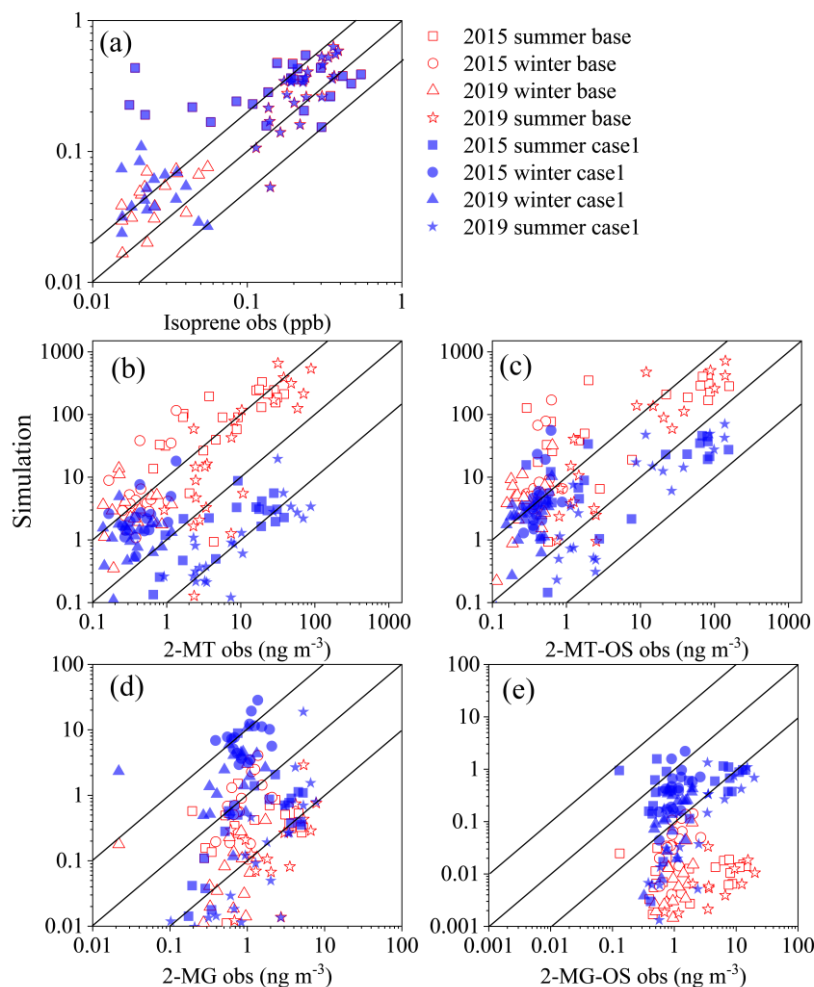
Figure 3. Comparisons of simulations against observations for (a) isoprene, (b) 2-MTs, (c) 2-MT-OS,

(d) 2-MG, (e) 2-MG-OS in summer and winter of 2015 and 2019. Red dot represents simulations with

standard CMAQ v5.2 (Base Case), and blue represents simulations using the optimized model (Case 1).

The 1:1, 10:1, and 1:10 lines are shown with solid lines.

The gas-phase and particle-phase fractions of 2-MG and 2-MTs were estimated using a chemical

equilibrium partitioning model as described in Section S3 and the results are shown in Figure S5. The

particle-phase fraction (F_p) of 2-MG was highly variable, with a significant lower value in summer (9.0

-19.0%) than in winter (31.6 - 44.0%), indicating substantial amounts of 2-MG was present in the gas

phase in summer. Additionally, the F_p value of iSOA polyols, in particular for 2-MG, decreased yearly.

As a result, the gas-plus-particle-phase concentrations of 2-MG showed an upward trend in summer

from 2015-2021 ($p < 0.05$, Figure S5). In contrast, 2-MTs were mainly distributed in the particle phase

with F_p values larger than 70% in both seasons, consistent with previous measurements (Isaacman-

467   Vanwertz et al., 2016). The inter-annual trend of 2-MTs was not significantly affected by their gas-phase

468   fraction because of the relatively low volatility. Overall, compared to other iSOA tracers in summer, 2-

469   MG and 2-MTs exhibited a distinctly different inter-annual trend over 2015-2021. It should be noted

470   that the use of surrogate standards would not alter the trend of iSOA tracers. The key factors driving

471   such trends will be discussed in detail below.

472   **3.3 Key influencing factors of iSOA formation**

473   The production of iSOA can be influenced by a variety of factors such as the emission and

474   concentration of isoprene, atmospheric oxidizing capacity as represented by the concentrations of O_3 or

475   odd oxygen ($O_x = O_3 + NO_2$), nitrogen oxides, as well as aerosol composition and properties including

476   sulfate content, acidity, and LWC. Here, we identify the major influencing factors of IEPOX-SOA and

477   HMML&MAE-SOA formation through the correlation analysis between different iSOA tracers and

478   influencing factors (Figure 4).

479   The correlations of all iSOA species with isoprene were relatively weak, with most of the

480   correlation coefficients (r^2) below 0.37. Therefore, the decline in iSOA concentrations from 2015 to

481   2021 could not be attributed to the slight variation in isoprene concentration. The HMML&MAE-SOA

482   species exhibited strong correlations with ozone ($r^2 = 0.48\text{-}0.81$) and O_x ($r^2 = 0.57\text{-}0.82$) in summer, in

483   particular in 2015 and 2021 while exhibiting relatively weaker correlations with NO_2 ($r^2 = 0.20\text{-}0.55$).

484   Such correlations between 2-MG and ozone were also observed in previous measurements in urban

485   areas in southeastern US (Rattanavaraha et al., 2016), which proposed that ozone might be a superior

486   indicator to NO_x for the photochemical process of isoprene under NO_x-dominant conditions. The

487   IEPOX-SOA tracers also correlated well with ozone ($r^2 = 0.36\text{-}0.70$) or O_x ($r^2 = 0.40\text{-}0.68$) in summer,

488   despite less strongly than HMML&MAE-SOA species. These observations clearly suggest that

489   atmospheric oxidation capacity (or the oxidation of isoprene to epoxide intermediates) plays a driving

490   role in summertime iSOA formation. In addition, weak to moderate correlations ($r^2 = 0.23\text{-}0.45$) were

491   observed between the iSOA tracers and sulfate aerosol in 2019 and 2021, indicating that sulfate aerosol

492   also plays a role in controlling iSOA formation during these periods. In contrast, wintertime iSOA

493   species exhibited weak correlations with O_3 and O_x in all the three years (Figure 4d-f). However, they

494   all had moderate or strong correlations with sulfate aerosol ($r^2 = 0.36\text{-}0.68$) in 2015 and the iSOA OSs

correlated moderately with sulfate (r^2 = 0.35-0.58) and LWC (r^2 = 0.34-0.58) in 2019 and 2021. These

results suggest that sulfate-mediated heterogeneous chemistry of isoprene epoxide intermediates in

aqueous aerosols is a key process controlling iSOA formation in winter (Surratt et al., 2010; Yee et al.,

2020; Lin et al., 2012). A sensitivity test considering the measurement uncertainties of iSOA tracers did

not significantly influence the correlation analysis results (see details in Section S5).
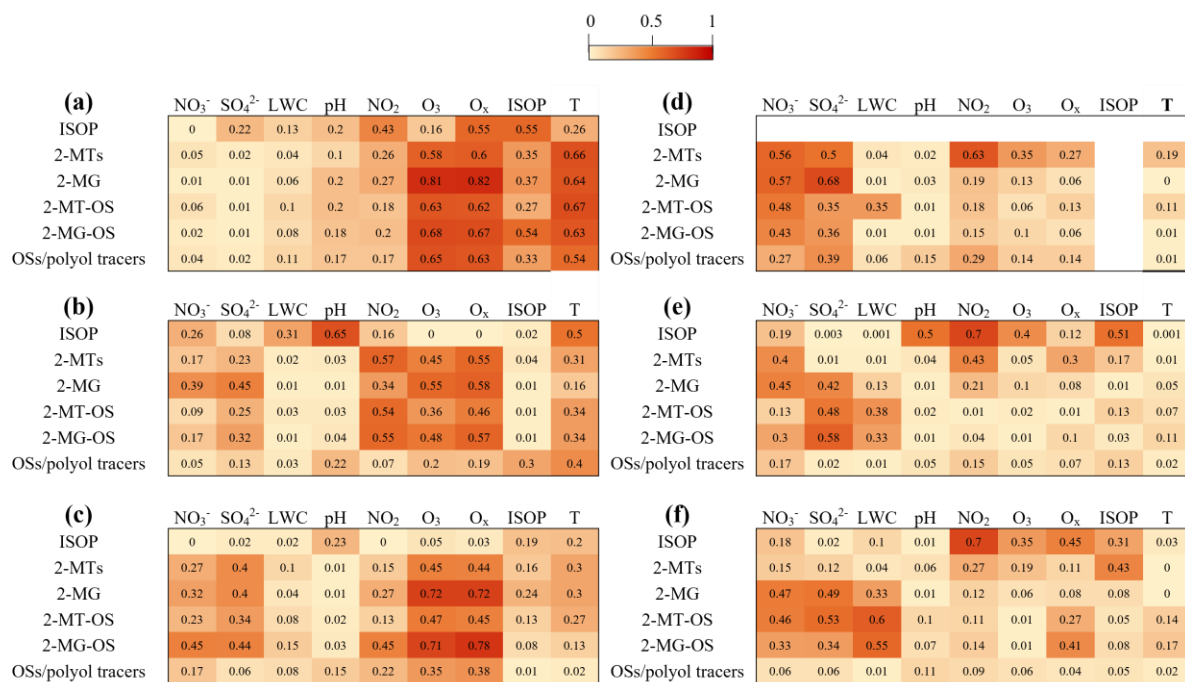
Figure 4. Coefficients of correlation (r^2) between iSOA compounds and various influencing factors of iSOA formation in (a-c) summer and (d-f) winter of 2015, 2019, and 2021, respectively. The ISOP is the abbreviation of isoprene.

As shown in Table S1, the concentrations of sulfate aerosol and LWC both decreased drastically

over 2015-2021 (p < 0.05), which could explain the declining trend of iSOA in winter and partially

contributed to the decreased formation of IEPOX-SOA in summer. Notably, the summertime average

MDA8 (maximum daily 8-h average) O_3 concentration at the observation site increased from 2015 to

2017 and then decreased significantly in 2018, followed by a slight increasing trend between 2018 and

2021 (Figure S6). This inter-annual trend of O_3 was similar to the trend of annual 90th percentile MDA8

O_3 concentration in the region of Shanghai (Figure S6). As a result, the summertime average MDA8 O_3

concentration in 2015, 2019, and 2021 showed a slight downward trend. In addition, the simulated

concentrations of OH radicals and ratios of (MVK+MACR)/isoprene both declined in 2019 compared

to those in 2015 (see Table S8), indicating a decline in the atmospheric oxidation capacity during the

observation period. Similarly, the nighttime atmospheric oxidation capacity as indicated by the production rate of NO_3 radicals (PNO$_3$), calculated by multiplying the reaction rate coefficient between NO_2 and O_3 by their concentrations (Wang et al., 2023), also decreased during this period (Figure S7). The reduced atmospheric oxidation capacity further explained the decreased formation of iSOA OSs in summer during these years, but it could not explain the inter-annual variation in summertime 2-MG and 2-MTs, suggesting that other factors might have offset the anticipated decline in these polyols during this period.

3.4 Heterogeneous reactivity of ambient aerosols

To better understand the role of heterogeneous chemistry in the formation and inter-annual variations of iSOA, the reactive uptake coefficients ($\gamma_{EPOXIDE}$) of isoprene-derived epoxides on ambient aerosols were estimated by a resistor model (eq. 4) (Xu et al., 2016; Pye et al., 2013). The pseudo-first-order heterogeneous reaction rate constant (k_{het}, s^{-1}) of gas-phase IEPOX and HMML&MAE could be then estimated from $\gamma_{EPOXIDE}$ via eq. 7. Currently, there are five sets of reported third-order reaction rate constants (i.e., $k_{i,j}$ in eq. 1) for the acid-catalyzed nucleophilic addition of water and sulfate to IEPOX in the aqueous phase (Table 1). Piletic et al. (2013) predicted $k_{i,j}$ for IEPOX ($k_{i,j\text{-IEPOX}}^{-1}$) with a computational model, which are two orders of magnitudes higher than the laboratory-measured values ($k_{i,j\text{-IEPOX}}^{-2}$) by Riedel et al. (2015) and model-estimated values ($k_{i,j\text{-IEPOX}}^{-3}$) using CMAQ by Pye et al. (2013). More recently, Pye et al. (2017) updated the values ($k_{i,j\text{-IEPOX}}^{-4}$) by constraining the $k_{i,j\text{-IEPOX}}^{-3}$ using measured 2-MT-OS/2-MTs in CMAQ and Chen et al. (2024) constrained reaction rate constant of IEPOX ($k_{i,j\text{-IEPOX}}^{-5}$) using a phase-separation box model with chamber measurements. For HMML and MAE, there is a lack of direct measurements and theoretical calculations of their $k_{i,j}$ values. Pye et al. (2013) assumed the same $k_{i,j}$ values as IEPOX with $k_{i,H+}$ of 9.0×10^{-4} M^{-2} s^{-1} for water and 2.0×10^{-4} M^{-2} s^{-1} for sulfate.

Table 1. Third-order reaction rate constants of IEPOX and HMML&MAE with sulfate and water in the aqueous phase

	k_{i,H^+} (M^{-2}·s^{-1})		k_{i,HSO_4^-} (M^{-2}·s^{-1})		References
	i=H$_2$O	i=SO$_4^{2-}$	i=H$_2$O	i=SO$_4^{2-}$	
$k_{i,j\text{-IEPOX}}$-1	5.3×10^{-2}	5.2×10^{-1}	—	—	(Piletic et al., 2013)
$k_{i,j\text{-IEPOX}}$ -2	3.4×10^{-4}	4.8×10^{-4}	—	—	(Riedel et al., 2015)
$k_{i,j\text{-IEPOX}}$ -3	9×10^{-4}	2×10^{-4}	1.3×10^{-5}	2.9×10^{-6}	(Pye et al., 2013)
$k_{i,j\text{-IEPOX}}$ -4	9×10^{-4}	8.8×10^{-3}	1.3×10^{-5}	2.9×10^{-6}	(Pye et al., 2017)
$k_{i,j\text{-IEPOX}}$ -5	5.3×10^{-4}	5.2×10^{-3}	—	—	(Chen et al., 2024)
$k_{i,j\text{-HMML\&MAE}}$	9×10^{-4}	2×10^{-4}	1.3×10^{-5}	2.9×10^{-6}	(Pye et al., 2013)

Firstly, the $k_{i,j}$ values of IEPOX and HMML&MAE were evaluated by comparing the measured ratios of 2-MT-OS/2-MTs and 2-MG-OS/2-MG with the calculated ratios of the pseudo-first-order rate constants for the nucleophilic addition reactions of epoxides with sulfate and water ($k_{aq,\,SO_4^{2-}}/k_{aq,\,H_2O}$). The results are shown in Figure S8 and S9. For IEPOX, the $k_{aq,\,SO_4^{2-}}/k_{aq,\,H_2O}$ ratios were close to measured particulate ratios of 2-MT-OS/2-MTs when using $k_{i,j\text{-IEPOX}}$-1, $k_{i,j\text{-IEPOX}}$-4, and $k_{i,j\text{-IEPOX}}$-5 suggested by Piletic et al. (2013), Pye et al. (2017), and Chen et al. (2024), respectively (Figure S8). However, when taking into account the underestimation of 2-MT-OS due to matrix effect, all estimated ratios were lower than the measured values. Similarly, the calculated $k_{aq,\,SO_4^{2-}}/k_{aq,\,H_2O}$ ratios for HMML and MAE were 1-2 orders of magnitude lower than the measured 2-MG-OS/2-MG ratios (Figure S9) and such a discrepancy would be larger when considering the matrix effect of 2-MG-OS. This result indicates that the k_{ij} of isoprene-derived epoxides, particularly that of HMML and MAE, with sulfate was likely underestimated, since Pye et al. (2013) found their hydrolysis rate constant allowed a good prediction of the concentration of 2-MG.

Figure 5 shows the γ and k_{het} values for IEPOX and HMML&MAE estimated using different sets of kinetic parameters listed in Table 1. The CMAQ-modeled values are also displayed for comparison. The k_{het} estimated by $k_{i,j\text{-IEPOX}}$-1, $k_{i,j\text{-IEPOX}}$-2 and $k_{i,j\text{-IEPOX}}$-5 in summer had highest values in 2019. This might be attributed to the fact that these three sets of parameters lack the third-order reaction rate constant of IEPOX with nucleophiles catalyzed by bisulfate (Table 1). As a comparison, we calculated

558   the k_{het} of IEPOX and HMML&MAE excluding the reaction rate constant catalyzed by bisulfate using

559   $k_{i,j\text{-IEPOX}}^{-3}$ and $k_{i,j\text{-IEPOX}}^{-4}$ (Figure S10). We found that the inter-annual trend of IEPOX (Figure S10a) and

560   HMML&MAE (Figure S10b) in summer was altered and similar to that of IEPOX calculated by $k_{i,j\text{-}}$

561   $_{\text{IEPOX}}^{-1}$, $k_{i,j\text{-IEPOX}}^{-2}$ and $k_{i,j\text{-IEPOX}}^{-5}$, while the inter-annual trend of k_{het} in winter was not sensitive to the

562   exclusion of reaction rate constant catalyzed by bisulfate. This result indicates a contribution of

563   nucleophilic-addition of epoxides catalyzed by bisulfate to the heterogeneous reactivity. It also suggests

564   that the $k_{i,j\text{-IEPOX}}^{-4}$ is more appropriate for predicting aerosol heterogeneous reactivity toward IEPOX

565   than other four sets of kinetic parameters.

566
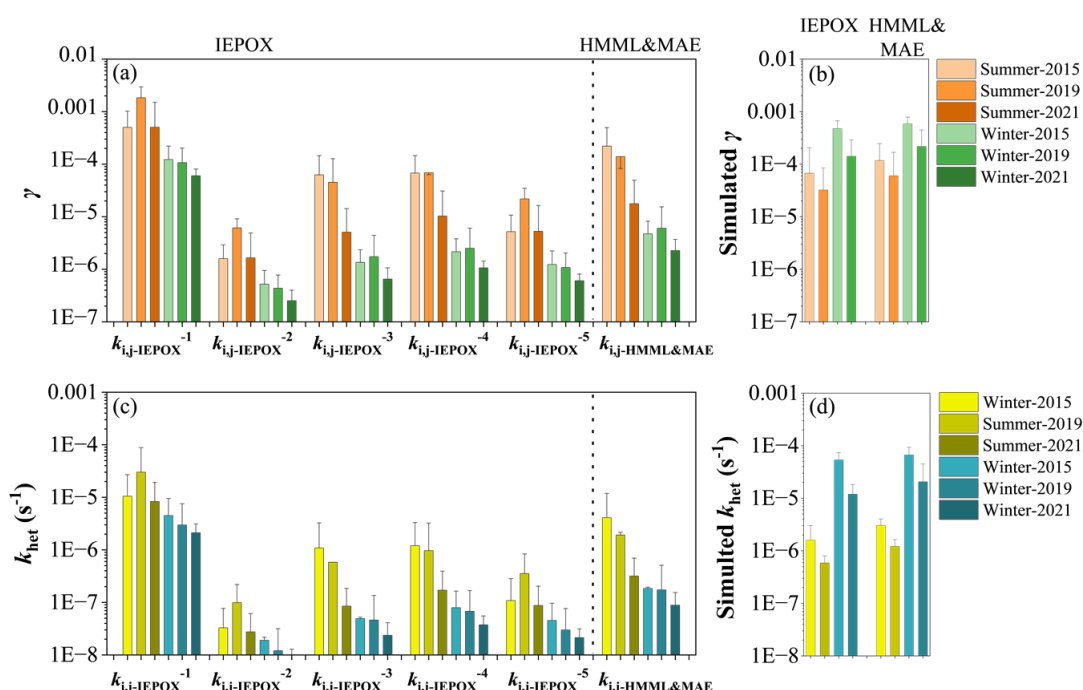
567   Figure 5. Reactive uptake coefficients (γ) and pseudo-first-order heterogeneous reaction rate constant

568   (k_{het}, s⁻¹) of gas-phase IEPOX and HMML&MAE estimated using different sets of $k_{i,j\text{-IEPOX}}$ and $k_{i,j\text{-}}$

569   $_{\text{HMML\&MAE}}$ listed in Table 1 (a and c) and simulated by CMAQ model in Case 1 (b and d).

570   As shown in Figure 5a and 5c, the estimated γ and k_{het} of IEPOX and HMML&MAE using $k_{i,j\text{-}}$

571   $_{\text{IEPOX}}^{-4}$ and $k_{i,j\text{-HMML\&MAE}}$ showed a similar trend which decreased in both winter and summer. Similar

572   decreasing trends in γ and k_{het} were also simulated by CMAQ (Figure 5b and 5d). The calculated γ and

573   k_{het} values of IEPOX and HMML&MAE in summer using $k_{i,j\text{-IEPOX}}^{-4}$ and $k_{i,j\text{--HMML\&MAE}}$, respectively, are

574   consistent with the simulated results, while the calculated values in winter were significantly lower than

575   the simulations, which is likely attributed to the significantly under-predicted aerosol pH and thereby

576 over-predicted aerosol reactivity in winter by the model. Overall, the declining trend of both calculated

577 and model-predicted k_{het} offers an explanation for the decreasing trend of 2-MT-OS and 2-MG-OS in

578 summer, but it could not explain the observed trend of 2-MG and 2-MTs in summer.

579 **3.5 Meteorological influences on iSOA variation**

580   As discussed above, the variations in chemical factors (including atmospheric oxidizing capacity

581 and aerosol heterogeneous reactivity) could well explain the declining trend of both summertime and

582 wintertime iSOA OSs, but not the trend of summertime 2-MG and 2-MTs during the period of 2015-

583 2021. Since meteorological conditions could exert a significant influence on the concentrations of

584 atmospheric pollutants (Liu et al., 2023b; Gu et al., 2023), we further investigate the impact of the

585 variation in meteorological conditions on the variation of iSOA during the observation period.

586   To do so, the CMAQ simulations for 2019 adopted the emissions of 2015 (Test Case), so the

587 variations in simulated iSOA concentration from 2015 to 2019 in this case is mainly attributed to the

588 changes in the meteorological conditions during these years. As shown in Figure 6, the simulated

589 variations in median concentrations of 2-MTs, 2-MT-OS, 2-MG, and 2-MG-OS in the Test case

590 accounted for 38.3-82.4% and 66.5-99.2% of the concentration reductions in Case 1 in summer and

591 winter, respectively. This suggests that the alteration in meteorological conditions exerts a more

592 substantial influence on the variation in iSOA concentrations compared to the changes in emissions.

593
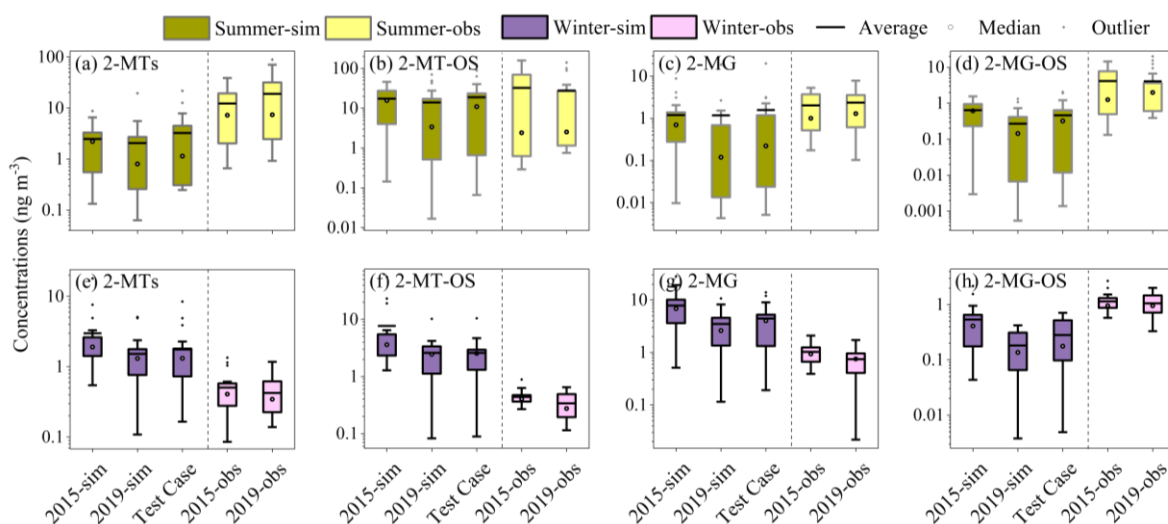
Figure 6. Simulated concentrations of 2-MTs, 2-MT-OS, 2-MG and 2-MG-OS in summer (a-d) and winter (e-h) in Case 1 (2015-sim and 2019-sim) and Test Case (simulations with 2015 emissions and 2019 meteorological conditions). The observed concentrations of 2-MTs, 2-MT-OS, 2-MG, and 2-MG-OS in 2015 and 2019 are also displayed (Detailed model-measurement comparisons are provided in Section 3.2; after accounting for matrix effect, 2-MT-OS would decrease more sharply and 2-MG-OS would show a descending inter-annual trend, consistent with model simulations).

It should be noted that the variations in meteorological conditions not only affect the physical processes such as dilution and transport, but also influence the chemical processes determining the formation of iSOA. To investigate the impacts of physical and chemical factors associated with the variations in meteorological conditions on the abundance of iSOA, the concentrations of elemental carbon (EC) were simulated in the Test Case. As shown in Figure 7, the simulated median concentrations of summertime and wintertime EC in 2019 both decreased by 32.8%, respectively, compared to those in 2015. Since EC is a primary pollutant and chemically inert under atmospheric conditions, the variations in its concentration in the Test Case is attributed to the changes in the physical processes, contributing approximately 59.5% of the EC reductions between 2015 and 2019 (Case 1). As a result, we could expect a similar contribution of the physical processes to the reduction in iSOA concentration. Notably, such reductions are significantly smaller than the simulated concentration reductions of iSOA in the Test case (Figure 6), suggesting that the chemical factors associated with the changes in meteorological conditions play a crucial role in determining the trend of iSOA in Shanghai,

consistent with the above analysis based on the observations. However, we note that the alternation in meteorological conditions cannot explain the observed non-declining trend of 2-MG and 2-MTs in summer, implying that some other factors that are not well represented in the CMAQ model may play a role in controlling such a trend.
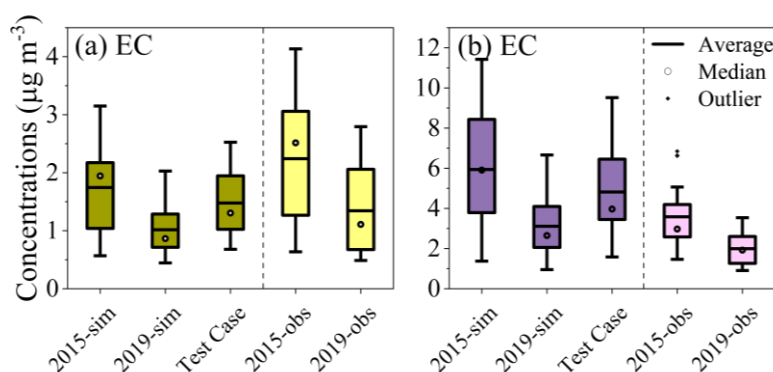
Figure 7. Simulated EC concentrations in Case 1 (2015-sim and 2019-sim) and Test Case (simulations with 2015 emissions and 2019 meteorological conditions) in (a) summer and (b) winter. The measured concentrations are also displayed and their trend is consistent with the simulations.

As discussed in Section 3.2, there is a large contribution of non-IEPOX sources to 2-MTs. Such sources might not be well represented in the model, which could explain the discrepancy between the simulated and observed trend of 2-MTs in summer. On the other hand, MACR is known as a first-generation oxidation product of isoprene and an important intermediate for iSOA formation through NOx-dominant pathways (Nguyen et al., 2015), but it can also originate from primary sources, such as biological emissions (Jardine et al., 2012), residential wood burning (Gaeggeler et al., 2008), and vehicle exhaust emissions (He et al., 2009). In certain urban areas, MACR arises primarily from vehicular emissions, as observed at the Heshan site in the Pearl River Delta region, China (Ling et al., 2019) and in Houston, US (Park et al., 2011). In the present work, the simulated MACR concentration demonstrated a decreasing trend from 2015 to 2019 in summer when the contribution of primary emissions was considered in the model. Yet, our recent study revealed that, despite a good agreement between modelled and measured isoprene concentrations, the model under-predicted the peak concentrations of MACR during the noon in urban Shanghai (Li et al., 2022), implying an underestimation of secondary formation and/or primary emissions of MACR in the model. Furthermore, Gu et al. (2023) reported that in the southern cities of Jiangsu Province, which is adjacent to Shanghai,

637   anthropogenic VOCs increased by approximately 15% from 2015 to 2019. Therefore, we infer that the

638   sources (e.g., primary emissions) of MACR might be under-predicted in this work, which may provide

639   a rationale for the inconsistency between simulated and observed inter-annual trends of 2-MG.

640   **4. Conclusions**

641   In this study, observations of isoprene-derived SOA species in ambient $PM_{2.5}$ were conducted at

642   an urban site in Shanghai, China during summer and winter in 2015, 2019, and 2021, aiming to

643   understand the response of biogenic SOA formation to anthropogenic emission reductions in polluted

644   regions. The complementary CMAQ model simulations were also performed for 2015 and 2019 and

645   the results are compared to the measurements. It is found that the particulate concentration of total iSOA

646   tracers, dominated by IEPOX-SOA species including 2-MT-OS and 2-MTs, had a decreasing trend from

647   2015 to 2021 (55.6, 51.0, and 29.7 ng m^{-3} in 2015, 2019, and 2021, respectively). When the

648   measurement uncertainties of iSOA tracers such as the matrix effect of OSs were considered, 2-MT-OS

649   and 2-MG-OS exhibited a declining trend in both seasons during the observation period. In contrast, 2-

650   MG and 2-MTs showed no significant inter-annual variations After accounting for the gas-phase

651   fraction, 2-MG even exhibited a slight upward trend in summer during these years.

652   The isoprene-derived SOA species correlated well with ozone and O_x in summer but with sulfate

653   in winter, suggesting that the atmospheric oxidation of isoprene to epoxide intermediates and their

654   subsequent reactive uptake on aqueous aerosols are the key steps driving the formation of iSOA in

655   summer and winter, respectively. The Ox-represented atmospheric oxidizing capacity and aerosol

656   heterogeneous reactivity decreased significantly during the observation period, which provided an

657   explanation for the decreasing trend of iSOA tracers in summer and winter (with the exception of

658   summertime 2-MG and 2-MTs).

659   The CMAQ model predicted the concentrations of iSOA tracers reasonably well and captured the

660   declining trend of total iSOA, 2-MT-OS, and 2-MG-OS in both seasons, but not the insignificant inter-

661   annual variations of 2-MG and 2-MTs in summer. Further model simulations show that inter-annual

662   variations in iSOA concentration are mainly governed by the changes in the meteorological conditions

663   rather than the emissions. Consistent with the analysis based on the observation data, the model

664   simulations show that the changes in chemical factors such as aerosol heterogeneous reactivity caused

665 by variations in meteorological conditions play an important role in controlling the inter-annual trend

666 of iSOA. The discrepancy between measured and modeled inter-annual trends of 2-MG and 2-MTs is

667 likely ascribed to the presence of unaccounted or underrepresented factors such as the direct emissions

668 of MACR and 2-MTs in the model. Overall, our study revealed the responses and underlying driving

669 factors of iSOA formation under rapidly changing anthropogenic emissions conditions in a typical

670 Chinese megacity. It also highlights the importance of tailored emission reductions for the mitigation

671 of PM formation from biogenic emissions through the regulation of atmospheric oxidizing capacity and

672 aerosol chemical reactivity.

673 **Data availability.**

674 The data presented in this work are available upon request from the corresponding author.

675 **Competing interests.**

676 The authors declare no competing interest relevant to this study.

677 **Author Contributions.**

678 YZ conceived and designed the study, HH, YW, and TY performed the field observation and analyzed

679 the data, JL, YL, TL, and YS performed the model simulations, HH, YZ, and JL wrote the paper, and

680 all other authors contributed to the discussion and writing.

681 **Acknowledgements.**

682 This study was supported by the National Key R&D Program of China (no. 2022YFC3701003) and the

683 National Natural Science Foundation of China (no. 22376137 and 22206120).

684 **References**

685 Bates, K. H., Crounse, J. D., St. Clair, J. M., Bennett, N. B., Nguyen, T. B., Seinfeld, J. H., Stoltz, B.
686   M., and Wennberg, P. O.: Gas Phase Production and Loss of Isoprene Epoxydiols, J. Phys. Chem.
687   A, 118, 1237-1246, 10.1021/jp4107958, 2014.

688 Bryant, D. J., Elzein, A., Newland, M., White, E., Swift, S., Watkins, A., Deng, W., Song, W., Wang, S.,
689   Zhang, Y., Wang, X., Rickard, A. R., and Hamilton, J. F.: Importance of Oxidants and Temperature
690   in the Formation of Biogenic Organosulfates and Nitrooxy Organosulfates, ACS Earth Space
691   Chem, 5, 2291-2306, 10.1021/acsearthspacechem.1c00204, 2021.

692 Bryant, D. J., Dixon, W. J., Hopkins, J. R., Dunmore, R. E., Pereira, K. L., Shaw, M., Squires, F. A.,
693   Bannan, T. J., Mehra, A., Worrall, S. D., Bacak, A., Coe, H., Percival, C. J., Whalley, L. K., Heard,
694   D. E., Slater, E. J., Ouyang, B., Cui, T., Surratt, J. D., Liu, D., Shi, Z., Harrison, R., Sun, Y., Xu,
695   W., Lewis, A. C., Lee, J. D., Rickard, A. R., and Hamilton, J. F.: Strong anthropogenic control of
696   secondary organic aerosol formation from isoprene in Beijing, Atmos. Chem. Phys., 20, 7531-
697   7552, 10.5194/acp-20-7531-2020, 2020.

698 Chen, Y., Ng, A. E., Green, J., Zhang, Y., Riva, M., Riedel, T. P., Pye, H. O. T., Lei, Z., Olson, N. E.,
699   Cooke, M. E., Zhang, Z., Vizuete, W., Gold, A., Turpin, B. J., Ault, A. P., and Surratt, J. D.:
700   Applying a Phase-Separation Parameterization in Modeling Secondary Organic Aerosol Formation
701   from Acid-Driven Reactive Uptake of Isoprene Epoxydiols under Humid Conditions, ACS ES&T
702   Air, 1, 511-524, 10.1021/acsestair.4c00002, 2024.

703 Cui, T., Zeng, Z., dos Santos, E. O., Zhang, Z., Chen, Y., Zhang, Y., Rose, C. A., Budisulistiorini, S. H.,
704   Collins, L. B., Bodnar, W. M., de Souza, R. A. F., Martin, S. T., Machado, C. M. D., Turpin, B. J.,
705   Gold, A., Ault, A. P., and Surratt, J. D.: Development of a hydrophilic interaction liquid
706   chromatography (HILIC) method for the chemical characterization of water-soluble isoprene
707   epoxydiol (IEPOX)-derived secondary organic aerosol, ENVIRON SCI-PROC IMP, 20, 1524-
708   1536, 10.1039/C8EM00308D, 2018.

709 Ding, X., He, Q. F., Shen, R. Q., Yu, Q. Q., and Wang, X. M.: Spatial distributions of secondary organic
710   aerosols from isoprene, monoterpenes, beta-caryophyllene, and aromatics over China during
711   summer, J Geophys Res-atmos, 119, 11877-11891, Doi 10.1002/2014jd021748, 2014.

712 Eddingsaas, N. C., VanderVelde, D. G., and Wennberg, P. O.: Kinetics and Products of the Acid-
713   Catalyzed Ring-Opening of Atmospherically Relevant Butyl Epoxy Alcohols, J. Phys. Chem. A,
714   114, 8106-8113, 10.1021/jp103907c, 2010.

715 Fan, Y., Liu, C.-Q., Li, L., Ren, L., Ren, H., Zhang, Z., Li, Q., Wang, S., Hu, W., Deng, J., Wu, L.,
716   Zhong, S., Zhao, Y., Pavuluri, C. M., Li, X., Pan, X., Sun, Y., Wang, Z., Kawamura, K., Shi, Z.,
717   and Fu, P.: Large contributions of biogenic and anthropogenic sources to fine organic aerosols in
718   Tianjin, North China, Atmos. Chem. Phys., 20, 117-137, 10.5194/acp-20-117-2020, 2020.

719 Frauenheim, M., Offenberg, J., Zhang, Z., Surratt, J. D., and Gold, A.: The C5–Alkene Triol Conundrum:
720   Structural Characterization and Quantitation of Isoprene-Derived $C_5H_{10}O_3$ Reactive Uptake
721   Products, Environ. Sci. Technol. Lett, 9, 829-836, 10.1021/acs.estlett.2c00548, 2022.

722 Frauenheim, M., Offenberg, J., Zhang, Z., Surratt, J. D., and Gold, A.: Chemical Composition of
723   Secondary Organic Aerosol Formed from the Oxidation of Semivolatile Isoprene Epoxydiol
724   Isomerization Products, Environ. Sci. Technol, 58, 22571-22582, 10.1021/acs.est.4c06850, 2024.

725 Fu, P., Aggarwal, S. G., Chen, J., Li, J., Sun, Y., Wang, Z., Chen, H., Liao, H., Ding, A., Umarji, G. S.,
726   Patil, R. S., Chen, Q., and Kawamura, K.: Molecular Markers of Secondary Organic Aerosol in
727   Mumbai, India, Environ Sci Technol, 50, 4659-4667, 10.1021/acs.est.6b00372, 2016.

728 Fu, P. Q., Kawamura, K., Chen, J., and Miyazaki, Y.: Secondary Production of Organic Aerosols from
729   Biogenic VOCs over Mt. Fuji, Japan, Environ Sci Technol, 48, 8491-8497, 10.1021/es500794d,
730   2014.

731 Fu, P. Q., Kawamura, K., Chen, J., Li, J., Sun, Y. L., Liu, Y., Tachibana, E., Aggarwal, S. G., Okuzawa,
732   K., Tanimoto, H., Kanaya, Y., and Wang, Z. F.: Diurnal variations of organic molecular tracers and
733   stable carbon isotopic composition in atmospheric aerosols over Mt. Tai in the North China Plain:
734   an influence of biomass burning, Atmos. Chem. Phys., 12, 8359-8375, 10.5194/acp-12-8359-2012,
735   2012.

736 Gaeggeler, K., Prevot, A. S. H., Dommen, J., Legreid, G., Reimann, S., and Baltensperger, U.:
737   Residential wood burning in an Alpine valley as a source for oxygenated volatile organic
738   compounds, hydrocarbons and organic acids, Atmos. Environ, 42, 8278-8287,
739   10.1016/j.atmosenv.2008.07.038, 2008.

740 Geng, G., Liu, Y., Liu, Y., Liu, S., Cheng, J., Yan, L., Wu, N., Hu, H., Tong, D., Zheng, B., Yin, Z., He,
741   K., and Zhang, Q.: Efficacy of China's clean air actions to tackle PM2.5 pollution between 2013
742   and 2020, Nat. Geosci, 17, 987-994, 10.1038/s41561-024-01540-z, 2024.

743 Gong, J., Yin, Z., Lei, Y., Lu, X., Zhang, Q., Cai, C., Chai, Q., Chen, H., Chen, R., Chen, W., Cheng, J.,
744   Chi, X., Dai, H., Dong, Z., Geng, G., Hu, J., Hu, S., Huang, C., Li, T., Li, W., Li, X., Lin, Y., Liu,
745   J., Ma, J., Qin, Y., Tang, W., Tong, D., Wang, J., Wang, L., Wang, Q., Wang, X., Wang, X., Wu, L.,
746   Wu, R., Xiao, Q., Xie, Y., Xu, X., Xue, T., Yu, H., Zhang, D., Zhang, L., Zhang, N., Zhang, S.,
747   Zhang, S., Zhang, X., Zhang, Z., Zhao, H., Zheng, B., Zheng, Y., Zhu, T., Wang, H., Wang, J., and
748   He, K.: The 2023 report of the synergetic roadmap on carbon neutrality and clean air for China:
749   Carbon reduction, pollution mitigation, greening, and growth, Environ. Sci. Ecotechnol., 23,
750   100517, https://doi.org/10.1016/j.ese.2024.100517, 2025.

751 Gu, C., Zhang, L., Xu, Z., Xia, S., Wang, Y., Li, L., Wang, Z., Zhao, Q., Wang, H., and Zhao, Y.: High-
752   resolution regional emission inventory contributes to the evaluation of policy effectiveness: a case
753   study in Jiangsu Province, China, Atmos. Chem. Phys., 23, 4247-4269, 10.5194/acp-23-4247-2023,
754   2023.

755 Guenther, A., Karl, T., Harley, P., Wiedinmyer, C., Palmer, P. I., and Geron, C.: Estimates of global
756   terrestrial isoprene emissions using MEGAN (Model of Emissions of Gases and Aerosols from
757   Nature), Atmos. Chem. Phys., 6, 3181-3210, 10.5194/acp-6-3181-2006, 2006.

758 Guo, H., Xu, L., Bougiatioti, A., Cerully, K. M., Capps, S. L., Hite Jr, J. R., Carlton, A. G., Lee, S. H.,
759   Bergin, M. H., Ng, N. L., Nenes, A., and Weber, R. J.: Fine-particle water and pH in the
760   southeastern United States, Atmos. Chem. Phys., 15, 5211-5228, 10.5194/acp-15-5211-2015, 2015.

761 He, C., Ge, Y. S., Tan, J. W., You, K. W., Han, X. K., Wang, J. F., You, Q. W., and Shah, A. N.:
762   Comparison of carbonyl compounds emissions from diesel engine fueled with biodiesel and diesel,
763   Atmos. Environ, 43, 3657-3661, 10.1016/j.atmosenv.2009.04.007, 2009.

Hennigan, C. J., Izumi, J., Sullivan, A. P., Weber, R. J., and Nenes, A.: A critical evaluation of proxy methods used to estimate the acidity of atmospheric particles, Atmos. Chem. Phys., 15, 2775-2790, 10.5194/acp-15-2775-2015, 2015.

Hettiyadura, A. P. S., Al-Naiema, I. M., Hughes, D. D., Fang, T., and Stone, E. A.: Organosulfates in Atlanta, Georgia: anthropogenic influences on biogenic secondary organic aerosol formation, Atmos. Chem. Phys., 19, 3191-3206, 10.5194/acp-19-3191-2019, 2019.

Hettiyadura, A. P. S., Stone, E. A., Kundu, S., Baker, Z., Geddes, E., Richards, K., and Humphry, T.: Determination of atmospheric organosulfates using HILIC chromatography with MS detection, Atmos. Meas. Tech., 8, 2347-2358, 10.5194/amt-8-2347-2015, 2015.

Hu, D., Bian, Q., Li, T. W. Y., Lau, A. K. H., and Yu, J. Z.: Contributions of isoprene, monoterpenes, β-caryophyllene, and toluene to secondary organic aerosols in Hong Kong during the summer of 2006, J Geophys Res-atmos, 113, https://doi.org/10.1029/2008JD010437, 2008.

Isaacman-VanWertz, G., Yee, L. D., Kreisberg, N. M., Wernis, R., Moss, J. A., Hering, S. V., de Sá, S. S., Martin, S. T., Alexander, M. L., Palm, B. B., Hu, W., Campuzano-Jost, P., Day, D. A., Jimenez, J. L., Riva, M., Surratt, J. D., Viegas, J., Manzi, A., Edgerton, E., Baumann, K., Souza, R., Artaxo, P., and Goldstein, A. H.: Ambient Gas-Particle Partitioning of Tracers for Biogenic Oxidation, Environ Sci Technol, 50, 9952-9962, 10.1021/acs.est.6b01674, 2016.

Jardine, K. J., Monson, R. K., Abrell, L., Saleska, S. R., Arneth, A., Jardine, A., Ishida, F. Y., Serrano, A. M. Y., Artaxo, P., Karl, T., Fares, S., Goldstein, A., Loreto, F., and Huxman, T.: Within-plant isoprene oxidation confirmed by direct emissions of oxidation products methyl vinyl ketone and methacrolein, Global Change Biol. , 18, 973-984, 10.1111/j.1365-2486.2011.02610.x, 2012.

Kang, M. J., Fu, P. Q., Kawamura, K., Yang, F., Zhang, H. L., Zang, Z. C., Ren, H., Ren, L. J., Zhao, Y., Sun, Y. L., and Wang, Z. F.: Characterization of biogenic primary and secondary organic aerosols in the marine atmosphere over the East China Sea, Atmos. Chem. Phys., 18, 13947-13967, 10.5194/acp-18-13947-2018, 2018.

Kelly, J. M., Doherty, R. M., O'Connor, F. M., and Mann, G. W.: The impact of biogenic, anthropogenic, and biomass burning volatile organic compound emissions on regional and seasonal variations in secondary organic aerosol, Atmos. Chem. Phys., 18, 7393-7422, 10.5194/acp-18-7393-2018, 2018.

Kjaergaard, H. G., Knap, H. C., Ørnsø, K. B., Jørgensen, S., Crounse, J. D., Paulot, F., and Wennberg, P. O.: Atmospheric fate of methacrolein. 2. Formation of lactone and implications for organic aerosol production, J Phys Chem A, 116, 5763-5768, 10.1021/jp210853h, 2012.

Kurokawa, J. and Ohara, T.: Long-term historical trends in air pollutant emissions in Asia: Regional Emission inventory in ASia (REAS) version 3, Atmos. Chem. Phys., 20, 12761-12793, 10.5194/acp-20-12761-2020, 2020.

Lewandowski, M., Piletic, I. R., Kleindienst, T. E., Offenberg, J. H., Beaver, M. R., Jaoui, M., Docherty, K. S., and Edney, E. O.: Secondary organic aerosol characterisation at field sites across the United States during the spring–summer period, Int J Environ Anal Chem, 93, 1084-1103, 10.1080/03067319.2013.803545, 2013.

Li, J., Xie, X., Li, L., Wang, X., Wang, H., Jing, S. a., Ying, Q., Qin, M., and Hu, J.: Fate of Oxygenated Volatile Organic Compounds in the Yangtze River Delta Region: Source Contributions and Impacts on the Atmospheric Oxidation Capacity, Environ Sci Technol, 56, 11212-11224, 10.1021/acs.est.2c00038, 2022.

Lin, Y. H., Zhang, H., Pye, H. O. T., Zhang, Z., Marth, W. J., Park, S., Arashiro, M., Cui, T., Budisulistiorini, S. H., and Sexton, K. G.: Epoxide as a precursor to secondary organic aerosol formation from isoprene photooxidation in the presence of nitrogen oxides, Proc. Natl. Acad. Sci., 110, 6718-6723, 2013.

Lin, Y. H., Zhang, Z. F., Docherty, K. S., Zhang, H. F., Budisulistiorini, S. H., Rubitschun, C. L., Shaw, S. L., Knipping, E. M., Edgerton, E. S., Kleindienst, T. E., Gold, A., and Surratt, J. D.: Isoprene Epoxydiols as Precursors to Secondary Organic Aerosol Formation: Acid-Catalyzed Reactive Uptake Studies with Authentic Compounds, Environ Sci Technol, 46, 250-258, 10.1021/es202554c, 2012.

Ling, Y., Wang, Y., Duan, J., Xie, X., Liu, Y., Peng, Y., Qiao, L., Cheng, T., Lou, S., Wang, H., Li, X., and Xing, X.: Long-term aerosol size distributions and the potential role of volatile organic compounds (VOCs) in new particle formation events in Shanghai, Atmos Environ, 202, 345-356, 10.1016/j.atmosenv.2019.01.018, 2019.

Liu, P., Ding, X., Bryant, D. J., Zhang, Y.-Q., Wang, J.-Q., Yang, K., Cheng, Q., Jiang, H., Wang, Z.-R., He, Y.-F., Li, B.-X., Zhao, M.-Y., Hamilton, J. F., Rickard, A. R., and Wang, X.-M.: Comparison of Isoprene-Derived Secondary Organic Aerosol Formation Pathways at an Urban and a Forest Site, ACS Earth Space Chem, 9, 1752-1767, 10.1021/acsearthspacechem.4c00398, 2025.

Liu, Y., Yang, X., Tan, J., and Li, M.: Concentration prediction and spatial origin analysis of criteria air pollutants in Shanghai, Environ. Pollut., 327, 121535, https://doi.org/10.1016/j.envpol.2023.121535, 2023a.

Liu, Y., Geng, G., Cheng, J., Liu, Y., Xiao, Q., Liu, L., Shi, Q., Tong, D., He, K., and Zhang, Q.: Drivers of Increasing Ozone during the Two Phases of Clean Air Actions in China 2013-2020, Environ Sci Technol, 57, 10.1021/acs.est.3c00054, 2023b.

McNeill, V. F., Woo, J. L., Kim, D. D., Schwier, A. N., Wannell, N. J., Sumner, A. J., and Barakat, J. M.: Aqueous-phase secondary organic aerosol and organosulfate formation in atmospheric aerosols: a modeling study, Environ Sci Technol, 46 15, 8075-8081, 2012.

Nguyen, T. B., Bates, K. H., Crounse, J. D., Schwantes, R. H., Zhang, X., Kjaergaard, H. G., Surratt, J. D., Lin, P., Laskin, A., Seinfeld, J. H., and Wennberg, P. O.: Mechanism of the hydroxyl radical

834   oxidation of methacryloyl peroxynitrate (MPAN) and its pathway toward secondary organic
835   aerosol formation in the atmosphere, PCCP, 17, 17914-17926, 10.1039/c5cp02001h, 2015.

836   Orlando, J. J., Tyndall, G. S., and Paulson, S. E.: Mechanism of the OH-initiated oxidation of
837   methacrolein, Geophys. Res. Lett, 26, 2191-2194, https://doi.org/10.1029/1999GL900453, 1999.

838   Park, C., Schade, G. W., and Boedeker, I.: Characteristics of the flux of isoprene and its oxidation
839   products in an urban area, J Geophys Res-atmos, 116, 10.1029/2011jd015856, 2011.

840   Paulot, F., Crounse, J. D., Kjaergaard, H. G., Kurten, A., St Clair, J. M., Seinfeld, J. H., and Wennberg,
841   P. O.: Unexpected Epoxide Formation in the Gas-Phase Photooxidation of Isoprene, Science, 325,
842   730-733, 10.1126/science.1172910, 2009.

843   Piletic, I. R., Edney, E. O., and Bartolotti, L. J.: A computational study of acid catalyzed aerosol
844   reactions of atmospherically relevant epoxides, Phys. Chem. Chem. Phys., 15, 18065-18076,
845   10.1039/c3cp52851k, 2013.

846   Pye, H. O. T., Pinder, R. W., Piletic, I. R., Xie, Y., Capps, S. L., Lin, Y.-H., Surratt, J. D., Zhang, Z.,
847   Gold, A., Luecken, D. J., Hutzell, W. T., Jaoui, M., Offenberg, J. H., Kleindienst, T. E.,
848   Lewandowski, M., and Edney, E. O.: Epoxide Pathways Improve Model Predictions of Isoprene
849   Markers and Reveal Key Role of Acidity in Aerosol Formation, Environ Sci Technol, 47, 11056-
850   11064, 10.1021/es402106h, 2013.

851   Pye, H. O. T., Murphy, B. N., Xu, L., Ng, N. L., Carlton, A. G., Guo, H., Weber, R., Vasilakos, P., Appel,
852   K. W., Budisulistiorini, S. H., Surratt, J. D., Nenes, A., Hu, W., Jimenez, J. L., Isaacman-VanWertz,
853   G., Misztal, P. K., and Goldstein, A. H.: On the implications of aerosol liquid water and phase
854   separation for organic aerosol mass, Atmos. Chem. Phys., 17, 343-369, 10.5194/acp-17-343-2017,
855   2017.

856   Qin, M., Wang, X., Hu, Y., Ding, X., Song, Y., Li, M., Vasilakos, P., Nenes, A., and Russell, A. G.:
857   Simulating Biogenic Secondary Organic Aerosol During Summertime in China, J Geophys Res-
858   atmos, 123, 11,100-111,119, https://doi.org/10.1029/2018JD029185, 2018.

859   Rattanavaraha, W., Chu, K., Budisulistiorini, S. H., Riva, M., Lin, Y. H., Edgerton, E. S., Baumann, K.,
860   Shaw, S. L., Guo, H., King, L., Weber, R. J., Neff, M. E., Stone, E. A., Offenberg, J. H., Zhang, Z.,
861   Gold, A., and Surratt, J. D.: Assessing the impact of anthropogenic pollution on isoprene-derived
862   secondary organic aerosol formation in PM2.5 collected from the Birmingham, Alabama, ground
863   site during the 2013 Southern Oxidant and Aerosol Study, Atmos. Chem. Phys., 16, 4897-4914,
864   10.5194/acp-16-4897-2016, 2016.

865   Riedel, T. P., Lin, Y. H., Zhang, Z., Chu, K., Thornton, J. A., Vizuete, W., Gold, A., and Surratt, J. D.:
866   Constraining condensed-phase formation kinetics of secondary organic aerosol components from
867   isoprene epoxydiols, Atmos. Chem. Phys., 16, 1245-1254, 10.5194/acp-16-1245-2016, 2016.

868 Riedel, T. P., Lin, Y.-H., Budisulistiorini, H., Gaston, C. J., Thornton, J. A., Zhang, Z., Vizuete, W., Gold,
869   A., and Surrattt, J. D.: Heterogeneous Reactions of Isoprene-Derived Epoxides: Reaction
870   Probabilities and Molar Secondary Organic Aerosol Yield Estimates, Environ. Sci. Technol. Lett.,
871   2, 38-42, 10.1021/ez500406f, 2015.

872 Shrivastava, M., Andreae, M. O., Artaxo, P., Barbosa, H. M. J., Berg, L. K., Brito, J., Ching, J., Easter,
873   R. C., Fan, J., Fast, J. D., Feng, Z., Fuentes, J. D., Glasius, M., Goldstein, A. H., Alves, E. G.,
874   Gomes, H., Gu, D., Guenther, A., Jathar, S. H., Kim, S., Liu, Y., Lou, S., Martin, S. T., McNeill, V.
875   F., Medeiros, A., de Sa, S. S., Shilling, J. E., Springston, S. R., Souza, R. A. F., Thornton, J. A.,
876   Isaacman-VanWertz, G., Yee, L. D., Ynoue, R., Zaveri, R. A., Zelenyuk, A., and Zhao, C.: Urban
877   pollution greatly enhances formation of natural aerosols over the Amazon rainforest, Nat. Commun,
878   10, 10.1038/s41467-019-08909-4, 2019.

879 Song, S., Gao, M., Xu, W., Shao, J., Shi, G., Wang, S., Wang, Y., Sun, Y., and McElroy, M. B.: Fine-
880   particle pH for Beijing winter haze as inferred from different thermodynamic equilibrium models,
881   Atmos. Chem. Phys., 18, 7423-7438, 10.5194/acp-18-7423-2018, 2018.

882 St. Clair, J. M., Rivera-Rios, J. C., Crounse, J. D., Knap, H. C., Bates, K. H., Teng, A. P., Jørgensen, S.,
883   Kjaergaard, H. G., Keutsch, F. N., and Wennberg, P. O.: Kinetics and Products of the Reaction of
884   the First-Generation Isoprene Hydroxy Hydroperoxide (ISOPOOH) with OH, J. Phys. Chem. A,
885   120, 1441-1451, 10.1021/acs.jpca.5b06532, 2016.

886 Stone, E. A., Nguyen, T. T., Pradhan, B. B., and Man Dangol, P.: Assessment of biogenic secondary
887   organic aerosol in the Himalayas, Environ. Chem. , 9, 263-272, https://doi.org/10.1071/EN12002,
888   2012.

889 Surratt, J. D., Chan, A., Eddingsaas, N. C., Chan, M. N., Loza, C. L., Kwan, A. J., Hersey, S. P., Flagan,
890   R. C., Wennberg, P. O., and Seinfeld, J. H.: Reactive intermediates revealed in secondary organic
891   aerosol formation from isoprene, Proc. Natl. Acad. Sci., 107, 6640-6645, 2010.

892 Surratt, J. D., Kroll, J. H., Kleindienst, T. E., Edney, E. O., Claeys, M., Sorooshian, A., Ng, N. L.,
893   Offenberg, J. H., Lewandowski, M., Jaoui, M., Flagan, R. C., and Seinfeld, J. H.: Evidence for
894   organosulfates in secondary organic aerosol, Environ Sci Technol, 41, 517-527,
895   10.1021/es062081q, 2007.

896 Tao, S., Lu, X., Levac, N., Bateman, A. P., Nguyen, T. B., Bones, D. L., Nizkorodov, S. A., Laskin, J.,
897   Laskin, A., and Yang, X.: Molecular Characterization of Organosulfates in Organic Aerosols from
898   Shanghai and Los Angeles Urban Areas by Nanospray-Desorption Electrospray Ionization High-
899   Resolution Mass Spectrometry, Environ Sci Technol, 48, 10993-11001, 10.1021/es5024674, 2014.

900 Teng, A. P., Crounse, J. D., and Wennberg, P. O.: Isoprene Peroxy Radical Dynamics, J.Am.Chem.Soc,
901   139, 5367-5377, 10.1021/jacs.6b12838, 2017.

Wang, H., Wang, H., Lu, X., Lu, K., Zhang, L., Tham, Y. J., Shi, Z., Aikin, K., Fan, S., Brown, S. S., and Zhang, Y.: Increased night-time oxidation over China despite widespread decrease across the globe, Nat. Geosci, 16, 217-223, 10.1038/s41561-022-01122-x, 2023.

Wang, M., Duan, Y., Xu, W., Wang, Q., Zhang, Z., Yuan, Q., Li, X., Han, S., Tong, H., Huo, J., Chen, J., Gao, S., Wu, Z., Cui, L., Huang, Y., Xiu, G., Cao, J., Fu, Q., and Lee, S.: Measurement report: Characterisation and sources of the secondary organic carbon in a Chinese megacity over 5 years from 2016 to 2020, Atmos. Chem. Phys., 22, 12789-12802, 10.5194/acp-22-12789-2022, 2022.

Wang, W., Wu, M. H., Li, L., Zhang, T., Liu, X. D., Feng, J. L., Li, H. J., Wang, Y. J., Sheng, G. Y., Claeys, M., and Fu, J. M.: Polar organic tracers in $PM_{2.5}$ aerosols from forests in eastern China, Atmos. Chem. Phys., 8, 7507-7518, 10.5194/acp-8-7507-2008, 2008.

Wang, Y., Zhao, Y., Wang, Y., Yu, J.-Z., Shao, J., Liu, P., Zhu, W., Cheng, Z., Li, Z., Yan, N., and Xiao, H.: Organosulfates in atmospheric aerosols in Shanghai, China: seasonal and interannual variability, origin, and formation mechanisms, Atmos. Chem. Phys., 21, 2959-2980, 10.5194/acp-21-2959-2021, 2021.

Wiedinmyer, C., Kimura, Y., McDonald-Buller, E. C., Emmons, L. K., Buchholz, R. R., Tang, W., Seto, K., Joseph, M. B., Barsanti, K. C., Carlton, A. G., and Yokelson, R.: The Fire Inventory from NCAR version 2.5: an updated global fire emissions model for climate and chemistry applications, Geosci. Model Dev., 16, 3873-3891, 10.5194/gmd-16-3873-2023, 2023.

Worton, D. R., Surratt, J. D., LaFranchi, B. W., Chan, A. W. H., Zhao, Y., Weber, R. J., Park, J.-H., Gilman, J. B., de Gouw, J., Park, C., Schade, G., Beaver, M., St Clair, J. M., Crounse, J., Wennberg, P., Wolfe, G. M., Harrold, S., Thornton, J. A., Farmer, D. K., Docherty, K. S., Cubison, M. J., Jimenez, J.-L., Frossard, A. A., Russell, L. M., Kristensen, K., Glasius, M., Mao, J., Ren, X., Brune, W., Browne, E. C., Pusede, S. E., Cohen, R. C., Seinfeld, J. H., and Goldsteint, A. H.: Observational Insights into Aerosol Formation from Isoprene, Environ Sci Technol, 47, 11403-11413, 10.1021/es4011064, 2013.

Xu, L., Middlebrook, A. M., Liao, J., de Gouw, J. A., Guo, H., Weber, R. J., Nenes, A., Lopez-Hilfiker, F. D., Lee, B. H., Thornton, J. A., Brock, C. A., Neuman, J. A., Nowak, J. B., Pollack, I. B., Welti, A., Graus, M., Warneke, C., and Ng, N. L.: Enhanced formation of isoprene-derived organic aerosol in sulfur-rich power plant plumes during Southeast Nexus, J Geophys Res-atmos, 121, 11,137-111,153, https://doi.org/10.1002/2016JD025156, 2016.

Xu, L., Guo, H., Boyd, C. M., Klein, M., Bougiatioti, A., Cerully, K. M., Hite, J. R., Isaacman-VanWertz, G., Kreisberg, N. M., Knote, C., Olson, K., Koss, A., Goldstein, A. H., Hering, S. V., de Gouw, J., Baumann, K., Lee, S.-H., Nenes, A., Weber, R. J., and Ng, N. L.: Effects of anthropogenic emissions on aerosol formation from isoprene and monoterpenes in the southeastern United States, Proc. Natl. Acad. Sci., 112, 37-42, doi:10.1073/pnas.1417609112, 2015.

Yan, K., Wang, J., Peng, R., Yang, K., Chen, X., Yin, G., Dong, J., Weiss, M., Pu, J., and Myneni, R. B.: HiQ-LAI: a high-quality reprocessed MODIS leaf area index dataset with better spatiotemporal

consistency from 2000 to 2022, Earth Syst. Sci. Data, 16, 1601-1622, 10.5194/essd-16-1601-2024, 2024.

Yao, Y., Wang, W., Ma, K., Tan, H., Zhang, Y., Fang, F., and He, C.: Transmission paths and source areas of near-surface ozone pollution in the Yangtze River delta region, China from 2015 to 2021, J. Environ. Manage., 330, 117105, https://doi.org/10.1016/j.jenvman.2022.117105, 2023.

Yee, L. D., Isaacman-VanWertz, G., Wernis, R. A., Kreisberg, N. M., Glasius, M., Riva, M., Surratt, J. D., de Sá, S. S., Martin, S. T., Alexander, M. L., Palm, B. B., Hu, W., Campuzano-Jost, P., Day, D. A., Jimenez, J. L., Liu, Y., Misztal, P. K., Artaxo, P., Viegas, J., Manzi, A., de Souza, R. A. F., Edgerton, E. S., Baumann, K., and Goldstein, A. H.: Natural and Anthropogenically Influenced Isoprene Oxidation in Southeastern United States and Central Amazon, Environ Sci Technol, 54, 5980-5991, 10.1021/acs.est.0c00805, 2020.

Zang, H., Zhao, Y., Huo, J., Zhao, Q., Fu, Q., Duan, Y., Shao, J., Huang, C., An, J., Xue, L., Li, Z., Li, C., and Xiao, H.: High atmospheric oxidation capacity drives wintertime nitrate pollution in the eastern Yangtze River Delta of China, Atmos. Chem. Phys., 22, 4355-4374, 10.5194/acp-22-4355-2022, 2022.

Zhang, J., Liu, J., Ding, X., He, X., Zhang, T., Zheng, M., Choi, M., Isaacman-VanWertz, G., Yee, L., Zhang, H., Misztal, P., Goldstein, A. H., Guenther, A. B., Budisulistiorini, S. H., Surratt, J. D., Stone, E. A., Shrivastava, M., Wu, D., Yu, J. Z., and Ying, Q.: New formation and fate of Isoprene SOA markers revealed by field data-constrained modeling, npj Clim. Atmos. Sci., 6, 69, 10.1038/s41612-023-00394-3, 2023.

Zhang, Y.-Q., Chen, D.-H., Ding, X., Li, J., Zhang, T., Wang, J.-Q., Cheng, Q., Jiang, H., Song, W., Ou, Y.-B., Ye, P.-L., Zhang, G., and Wang, X.-M.: Impact of anthropogenic emissions on biogenic secondary organic aerosol: observation in the Pearl River Delta, southern China, Atmos. Chem. Phys., 19, 14403-14415, 10.5194/acp-19-14403-2019, 2019.

Zhang, Y.-Q., Ding, X., He, Q.-F., Wen, T.-X., Wang, J.-Q., Yang, K., Jiang, H., Cheng, Q., Liu, P., Wang, Z.-R., He, Y.-F., Hu, W.-W., Wang, Q.-Y., Xin, J.-Y., Wang, Y.-S., and Wang, X.-M.: Observational Insights into Isoprene Secondary Organic Aerosol Formation through the Epoxide Pathway at Three Urban Sites from Northern to Southern China, Environ Sci Technol, 10.1021/acs.est.1c06974, 2022.

Zheng, B., Tong, D., Li, M., Liu, F., Hong, C., Geng, G., Li, H., Li, X., Peng, L., Qi, J., Yan, L., Zhang, Y., Zhao, H., Zheng, Y., He, K., and Zhang, Q.: Trends in China's anthropogenic emissions since 2010 as the consequence of clean air actions, Atmos. Chem. Phys., 18, 14095-14111, 10.5194/acp-18-14095-2018, 2018.

Zhong, Y., Chen, J., Zhao, Q., Zhang, N., Feng, J., and Fu, Q.: Temporal trends of the concentration and sources of secondary organic aerosols in $PM_{2.5}$ in Shanghai during 2012 and 2018, Atmos. Environ, 261, 118596, https://doi.org/10.1016/j.atmosenv.2021.118596, 2021.

975 Zhou, M., Zheng, G., Wang, H., Qiao, L., Zhu, S., Huang, D., An, J., Lou, S., Tao, S., Wang, Q., Yan,
976   R., Ma, Y., Chen, C., Cheng, Y., Su, H., and Huang, C.: Long-term trends and drivers of aerosol
977   pH in eastern China, Atmos. Chem. Phys., 22, 13833-13844, 10.5194/acp-22-13833-2022, 2022.
978